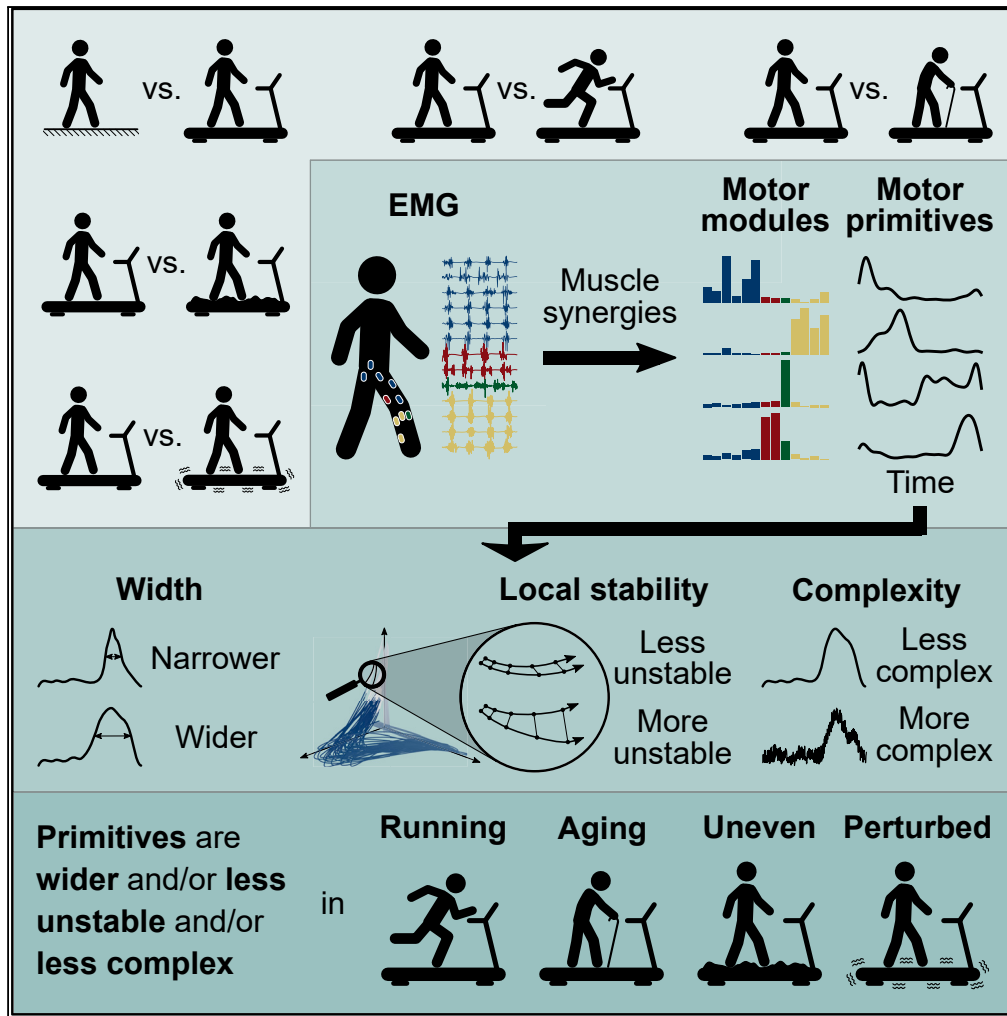**Article**

Neuromotor Dynamics of Human Locomotion in Challenging Settings

Alessandro
Santuz, Leon Brüll,
Antonis Ekizos, ...,
Armin Kibele,
Michael Schwenk,
Adamantios
Arampatzis

alessandro.santuz@hu-berlin.
de

HIGHLIGHTS
We examined the
dynamics of motor control
of locomotion in
challenging settings

We extracted muscle
synergies (motor modules
and primitives) from
electromyography

The dynamics of the time-
dependent motor
primitives were modified
by perturbations

Primitives were wider, less
unstable, and complex in
the presence of
perturbations

iScience

Article

Neuromotor Dynamics of Human Locomotion in Challenging Settings

Alessandro Santuz,[1,2,3,8,9,*] Leon Brüll,[1,2,4] Antonis Ekizos,[1,2] Arno Schroll,[1,2] Nils Eckardt,[5,6] Armin Kibele,[5] Michael Schwenk,[4,7] and Adamantios Arampatzis[1,2]

SUMMARY

Is the control of movement less stable when we walk or run in challenging settings? Intuitively, one might answer that it is, given that challenging locomotion externally (e.g., rough terrain) or internally (e.g., age-related impairments) makes our movements more unstable. Here, we investigated how young and old humans synergistically activate muscles during locomotion when different perturbation levels are introduced. Of these control signals, called _muscle synergies_, we analyzed the local stability and the complexity (or irregularity) over time. Surprisingly, we found that perturbations force the central nervous system to produce muscle activation patterns that are less unstable and less complex. These outcomes show that robust locomotion control in challenging settings is achieved by producing less complex control signals that are more stable over time, whereas easier tasks allow for more unstable and irregular control.

INTRODUCTION

The central nervous system (CNS), as the fundamental nonlinear component of the majority of animals, contains both deterministic and stochastic elements (Faisal et al., 2008; Rabinovich and Abarbanel, 1998). In behaviors such as locomotion, small variations in the initial conditions might generate big variations in the evolution of the system (Lorenz, 1963). Noise affects neural control signals by adding stochastic (i.e., random) disturbances in a signal-dependent manner: if the magnitude of the control signal increases, noise levels increase as well (Harris and Wolpert, 1998). To organize robust movement patterns, the CNS must handle deterministic and stochastic variables (Faisal et al., 2008; Rabinovich and Abarbanel, 1998). Defining robustness as the ability to cope with perturbations (Santuz et al., 2018a), it follows that biological systems can manage to maintain function despite disturbances only through robust control (Kitano, 2004; Meghdadi, 2004; Shinar and Feinberg, 2010). Assessing the local stability, which is the sensitivity to infinitesimally small perturbations (Lorenz, 1963), of control signals could give us an idea of the strategies adopted by the CNS to cope with disruptions, whether they are internal (e.g., aging or disease) or external (e.g., environmental, such as changes in the morphology of terrain). This is a different kind of stability when compared with the global one. Humans are _locally_ unstable due to the step-to-step variability of their movements but are at the same time _globally_ stable (i.e., the variations remain within the basin of attraction) if they manage to locomote without major disruptions (Ali and Menzinger, 1999; Dingwell and Hyun, 2007; Wisse et al., 2005).

With this study, we propose an innovative approach to describe the local dynamic stability (Bradley and Kantz, 2015; Dingwell and Cusumano, 2000; Lorenz, 1963) of human motor control applied to locomotion. We started from a crucial question: how is the local stability of control signals associated to robust motor output? The answer might give important insight into the neural mechanisms necessary for the robust control of vertebrate locomotion.

Despite its nonlinear behavior, the output of the CNS can be reasonably described and modeled by means of linear approximations (Bizzi et al., 2008). The overwhelming amount of degrees of freedom available to vertebrates for accomplishing any kind of movement is defined by the vast number of muscles and joints. Yet, the CNS manages to overcome complexity, possibly through the orchestrated activation of functionally related muscle groups, rather than through muscle-specific commands (Bernstein, 1967; Bizzi et al., 1991). These common activation patterns, called _muscle synergies_, might be used by the CNS for simplifying the motor control problem by reducing its dimensionality (Bizzi et al., 2008). Usually extracted from electromyographic (EMG) data via linear machine learning approaches such as the non-negative matrix factorization (NMF), muscle synergies have been increasingly employed in the past two decades for

[1]Department of Training and Movement Sciences, Humboldt-Universität zu Berlin, 10115 Berlin, Germany

[2]Berlin School of Movement Science, Humboldt-Universität zu Berlin, 10115 Berlin, Germany

[3]Atlantic Mobility Action Project, Brain Repair Centre, Department of Medical Neuroscience, Dalhousie University, Halifax, Nova Scotia B3H 4R2, Canada

[4]Network Aging Research, Heidelberg University, 69117 Heidelberg, Germany

[5]Department of Training and Movement Science, Institute for Sport and Sports Science, University of Kassel, 34125 Kassel, Germany

[6]Department of Sport and Movement Science, Institute of Sport Science, Carl von Ossietzky University of Oldenburg, 26129 Oldenburg, Germany

[7]Institute of Sports and Sports Sciences, Heidelberg University, 69117 Heidelberg, Germany

[8]Twitter: @alesantuz

[9]Lead Contact

*Correspondence: alessandro.santuz@hu-berlin.de

https://doi.org/10.1016/j.isci.2019.100796

providing indirect evidence of a simplified, modular control of movement in humans and other vertebrates (Giszter, 2015; Lacquaniti et al., 2012; Ting et al., 2015; Tresch et al., 1999).

We quantified the local dynamic stability of motor primitives (i.e., the temporal components of muscle synergies) in different locomotor tasks and settings by means of the short-term maximum Lyapunov exponents (sMLE), a metric used to describe the rate of separation of infinitesimally close trajectories (Rosenstein et al., 1993). Moreover, we used the Higuchi's fractal dimension (HFD) to evaluate the complexity of motor primitives, considered as self-similar time series (Higuchi, 1988). Namely, we considered what happens in the space of muscle synergies when humans switch from walking to running, from overground to treadmill locomotion, from unperturbed to perturbed locomotion, and in aging. We chose these conditions to compare different challenges or constraints to locomotion: running allows less time for organizing coordinated movements than walking (Ekizos et al., 2018); externally perturbed locomotion is more challenging than unperturbed locomotion due to the increased mechanical and physiological limits imposed by the higher environmental complexity (Daley, 2016; Santuz et al., 2018a); aging is a source of internal perturbation that leads to muscle weakness and loss of fine neural control at various levels (e.g., CNS, proprioceptive, etc.) (Monaco et al., 2010; Nutt et al., 1993). Recently, we and others proposed that the width of motor primitives increases to ensure robust control in the presence of internal and external perturbations (Cappellini et al., 2016; Martino et al., 2015, 2014; Santuz et al., 2019, 2018a). Martino and colleagues were the first to interpret the widening of motor primitives as a compensatory mechanism adopted by the CNS to cope with the postural instability of locomotion in health and pathology (Martino et al., 2015, 2014). We observed this neural strategy in wild-type mice (Santuz et al., 2019) and in humans (Santuz et al., 2018a) undergoing external perturbations, but not in genetically modified mice that lacked feedback from proprioceptors (Santuz et al., 2019). Owing to these observations, we concluded that intact systems use wider (i.e., of longer duration) control signals to create an overlap between chronologically adjacent synergies to regulate motor function (Santuz et al., 2018a). Our conclusions, however, did not include any information about the local stability and complexity of the control signals, eventually limiting the understanding of the adaptive processes needed to cope with perturbations.

With the present analysis of human data, we discovered that less unstable and less complex motor primitives are associated with more challenging settings, whereas easier tasks allow for more unstable and more complex control. Our findings provide insight into how our CNS might control repetitive, highly stereotyped movements like locomotion, in the presence and absence of perturbations. Moreover, these results add interesting aspects to the definition of robust motor control that we and others (Aoi et al., 2019; Santuz et al., 2018a) gave in the past, integrating the concepts of local stability and complexity with the width of control signals.

RESULTS

Muscle Synergies

Muscle synergies for human locomotion have been extensively discussed and reported in the past (Cappellini et al., 2006; Ivanenko et al., 2004; Lacquaniti et al., 2012; Martino et al., 2015; Santuz et al., 2018a, 2018b, 2017a, 2017b). Figure 1 shows a typical output for walking, where four fundamental synergies describe as many phases of the gait cycle. In human locomotion, the first synergy functionally refers to the body weight acceptance, with a major involvement of knee extensors and glutei. The second synergy describes the propulsion phase, to which the plantarflexors mainly contribute. The third synergy identifies the early swing, showing the involvement of foot dorsiflexors. The fourth and last synergy reflects the late swing and the landing preparation, highlighting the relevant influence of knee flexors and foot dorsiflexors.

Details about the participants are reported in the Supplemental Information. Briefly, the first group (G1) of young participants was assigned to the first experimental protocol (E1) consisting of walking and running overground and on a treadmill. The second group (G2) was assigned to the second experimental protocol (E2) consisting of walking and running on one standard and one uneven-surface (Figure S1, Video S1) treadmill. The last two groups (G3, young and G4, old) were assigned to the third and last protocol (E3) consisting of walking on a treadmill (Video S1) providing mediolateral and anteroposterior perturbations.

The minimum number of synergies that best accounted for the EMG data variance (i.e., the factorization rank) of E1 was 4.6 ± 0.5 (G1, overground walking), 4.6 ± 0.6 (G1, treadmill walking), 4.2 ± 0.7 (G1, overground running), and 4.6 ± 0.7 (treadmill running), with no significant main effects of locomotion type or
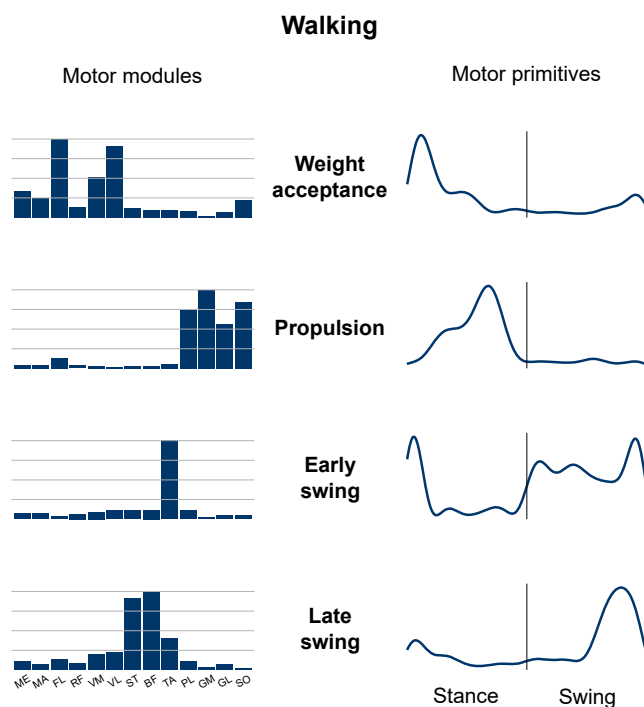
Walking

Motor modules   Motor primitives

Figure 1. Muscle Synergies for Human Walking

Exemplary motor modules and motor primitives of the four fundamental synergies for human walking (average of even-surface trials of the experimental setup E2). The motor modules are presented on a normalized y axis base. For the motor primitives, the x axis full scale represents the averaged gait cycle (with stance and swing normalized to the same amount of points and divided by a vertical line) and the y axis represents the normalized amplitude. Muscle abbreviations: ME, gluteus medius; MA, gluteus maximus; FL, tensor fasciæ latæ; RF, rectus femoris; VM, vastus medialis; VL, vastus lateralis; ST, semitendinosus; BF, biceps femoris; TA, tibialis anterior; PL, peroneus longus; GM, gastrocnemius medialis; GL, gastrocnemius lateralis; SO, soleus.

condition. In E2, the values were 4.7 ± 0.7 (G2, even-surface walking), 5.1 ± 0.6 (G2, uneven-surface walking), 4.2 ± 0.6 (G2, even-surface running), and 4.6 ± 0.6 (G2, uneven-surface running), with running showing significantly less synergies than walking (p = 0.005) and no statistically significant effect of surface. Finally, in E3 the factorization ranks were 4.5 ± 0.6 (G3, unperturbed walking, young), 4.9 ± 0.5 (G3, perturbed walking, young), 4.5 ± 0.6 (G4, unperturbed walking, old), and 4.6 ± 0.5 (G4, perturbed walking, old), with perturbed walking in the young showing significantly more synergies (p < 0.001).

Gait Cycle Parameters

The average stance and swing times together with the cadence are reported in Table 1. A main effect of speed (walking compared with running) was found in E1 and E2 for all parameters (p < 0.001) except for the swing time in E2 (p = 0.583). Treadmill, when compared with overground locomotion, made swing times decrease (p = 0.020). External perturbations (E2 and E3) influenced the stance, swing, and cadence in E3 (p < 0.001). Age played a significant role in reducing the swing times in older adults (p < 0.001). All the other comparisons were statistically (p > 0.05) not significant, and there were no interaction effects (p > 0.05).

Perturbations Make Motor Primitives Less Unstable, Less Complex, and Fuzzier

We analyzed motor primitives in their own space, the dimension of which was equal to the trial-specific number of synergies. Two representative trials factorized into three synergies each are plotted in three-dimensional graphs in Figure 2. We used the three-dimensional example because a space in more than three dimensions would be difficult to represent. We found that motor primitives were less unstable (i.e., show lower sMLE) in (1) running compared with walking, (2) perturbed compared with unperturbed locomotion, and (3) old compared with young participants (Figures 3 and S3). Motor primitives did not show any difference in the sMLE when comparing overground with treadmill locomotion. The HFD of motor

Experiment	Condition 1	Condition 2	Stance (ms)	Swing (ms)	Cadence (steps/min)
E1	Walking	Overground	689 ± 41	393 ± 26	111 ± 5
		Treadmill	674 ± 41	382 ± 30	114 ± 6
	Running	Overground	289 ± 27	473 ± 42	158 ± 11
		Treadmill	293 ± 27	449 ± 50	162 ± 12
E2	Walking	Even surface	674 ± 37	431 ± 29	109 ± 5
		Uneven surface	668 ± 49	437 ± 33	109 ± 7
	Running	Even surface	353 ± 50	424 ± 54	155 ± 7
		Uneven surface	324 ± 41	433 ± 53	159 ± 10
E3	Young	Normal walking	697 ± 32	403 ± 22	109 ± 4
		Perturbed walking	645 ± 28	377 ± 19	118 ± 5
	Old	Normal walking	693 ± 53	383 ± 23	111 ± 7
		Perturbed walking	645 ± 51	353 ± 26	121 ± 8

Table 1. Gait Spatiotemporal Parameters
Stance and swing times together with the cadence are reported for the three experimental setups (values ± standard deviation).

primitives are reported in Figure 4. In summary, we found that motor primitives were less complex (i.e., less irregular or with a lower fractal dimension) in (1) running compared with walking, (2) treadmill compared with overground walking, (3) overground compared with treadmill running, and (4) perturbed compared with unperturbed locomotion with older adults showing a smaller decrease in complexity than young when transitioning from unperturbed to perturbed walking (Figure 4).

In Table 2 we report synergy-by-synergy and for the three experimental setups, the factors that contributed to widen the motor primitives, thus increasing their temporal fuzziness. Detailed boxplots are available in Figure S2. Our findings show that a widening of the motor primitives, measured with the full width at half maximum (FWHM), can be observed in (1) running compared with walking, (2) perturbed compared with unperturbed locomotion, and (3) old compared with young participants (Table 2).

DISCUSSION

Historically, the sMLE have been used to give information about the behavior of chaotic dynamical systems (Dingwell and Cusumano, 2000; Ekizos et al., 2018, 2017; Kibushi et al., 2018; Santuz et al., 2018a). In this study, we described the local stability and complexity of modular motor control in humans by calculating the sMLE and HFD of motor primitives (i.e., the time-dependent coefficients of muscle synergies) during locomotion (walking and running) overground and on a treadmill, with or without external perturbations and in aging. Our results show lower local instability (i.e., lower sMLE), lower complexity (i.e., lower HFD), and longer basic activation patterns (i.e., higher FWHM) associated with aging, external perturbations, and the switch from walking to running.

We proposed an innovative and simple approach to describe the behavior over time of neural system modularity, with an eye on increasing the reproducibility of results (all the data and code are available at Zenodo, https://doi.org/10.5281/zenodo.2669485). Typically, the sMLE are calculated from data expanded in the state space, which is a set of all the possible states of a system at any given time (Lorenz, 1963; Packard et al., 1980; Rabinovich and Abarbanel, 1998). The main assumption underlying our method is that the analysis must be conducted in the muscle synergies space, with its own dimension that is equal to the factorization rank (i.e., the minimum number of synergies necessary to sufficiently reconstruct the original EMG signals). By doing so, we did not model the whole system dynamics, but focused on the modular behavior of the CNS. In this assumption lies also the high reproducibility of our approach, because this simplification of the calculations avoids two well-known weaknesses (Bradley and Kantz, 2015) of the classical approach: the choice of time delay, which is not needed here, and state space dimension, which is calculated by NMF, for delay embedding.
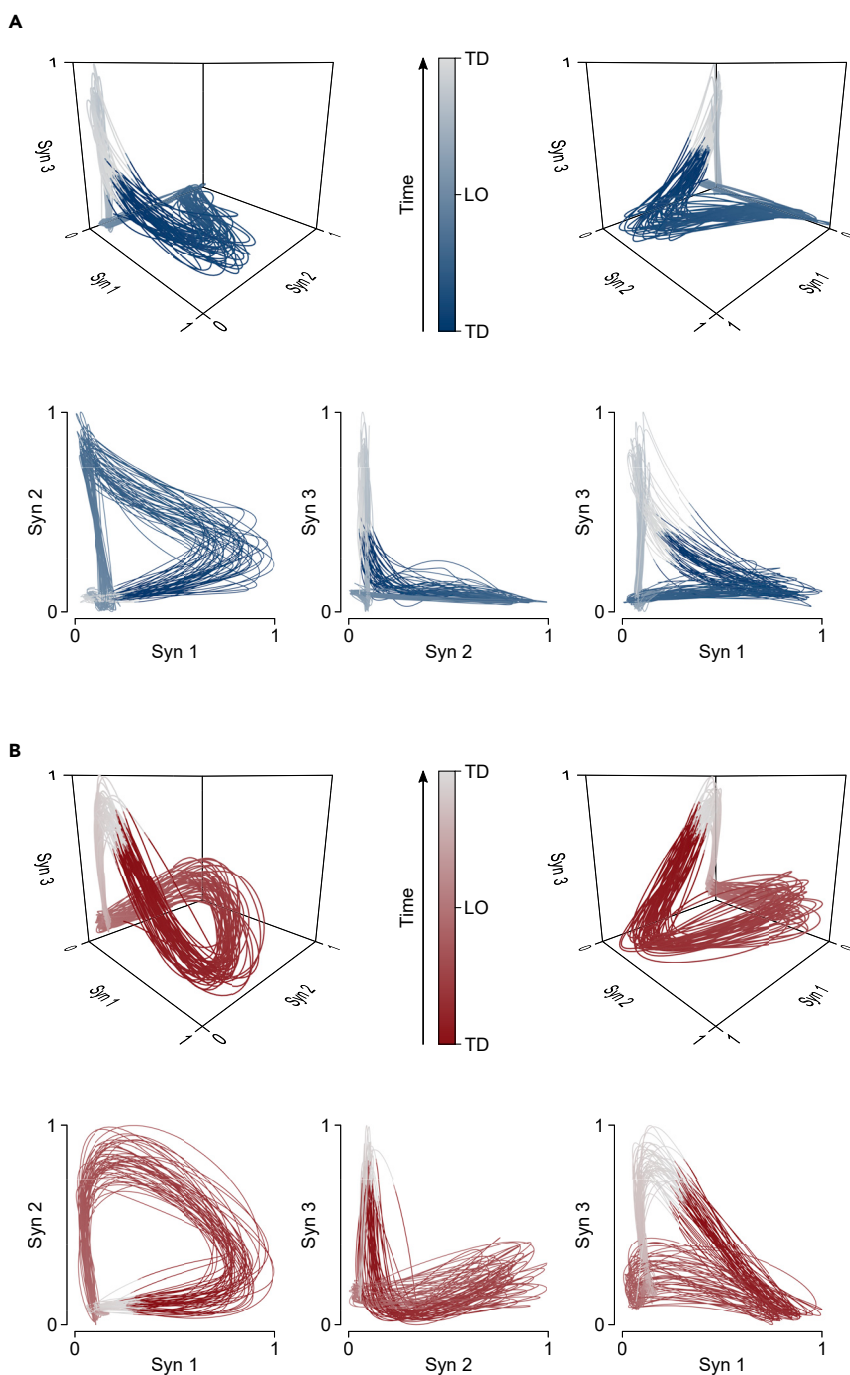
**Figure 2. Motor Primitive Trajectories in Their Own Space**

(A and B) Representative data showing the filtered trajectories of motor primitives when the number of synergies (Syn) is equal to three. (A) Blue curves refer to an unperturbed walking trial recorded from a young participant. (B) Red curves refer to an unperturbed running trial recorded from a young participant. Trajectories are color coded from touchdown (TD, dark blue or red), to lift-off (LO, light blue or red), to the next TD (white). The amplitude of motor primitives is normalized to the maximum value of each trial for better visualization.

HFD as a measure of irregularity or complexity has been proposed in 1988 (Higuchi, 1988) and recently re-discovered by neurophysiologists, especially for the study of electroencephalographic patterns (Kesić and Spasić, 2016; Smits et al., 2016; Zappasodi et al., 2014). Fractal time series repeat themselves at various
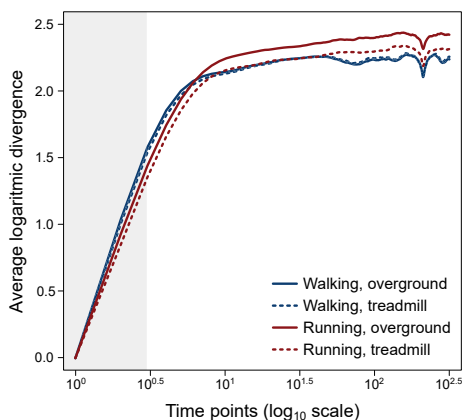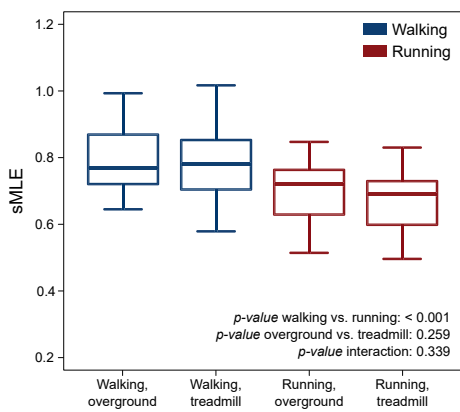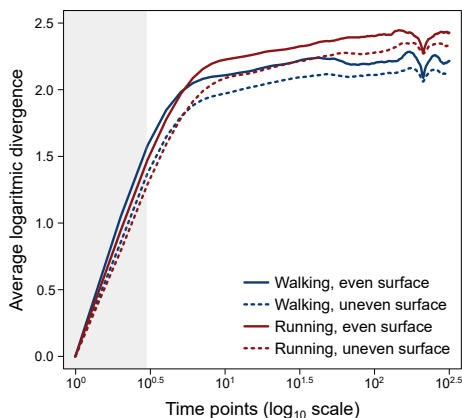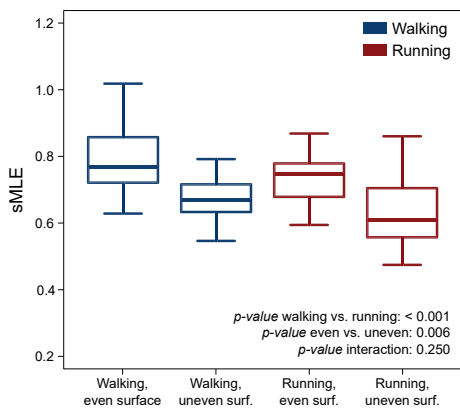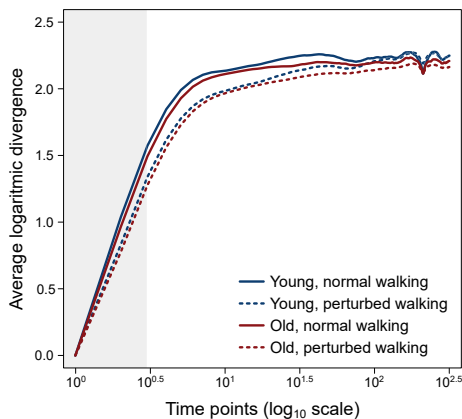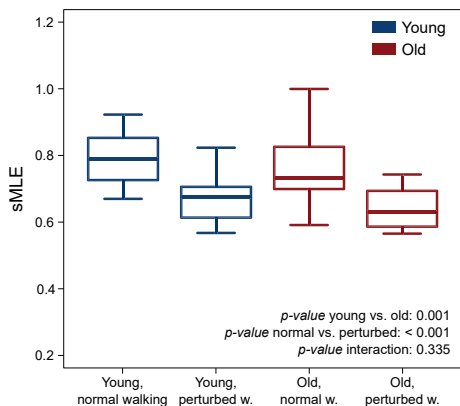
Figure 3. Short-Term Maximum Lyapunov Exponents of Motor Primitives

Boxplots and curves describing the short-term maximum Lyapunov exponents (sMLE) and the average logarithmic divergence curves for the three experimental setups (E1, walking and running, overground and treadmill; E2, walking and running, even and uneven surface; E3, young and old, unperturbed and perturbed walking). The minimum value was subtracted from each curve for improving the visualization. The actual vertical intercept was negative and different for all curves (Figure S3). The shaded area represents the portion considered for calculating the slope. Time is presented in $\log_{10}$ scale to highlight the curve slopes. Lower sMLE imply less locally unstable motor primitives.
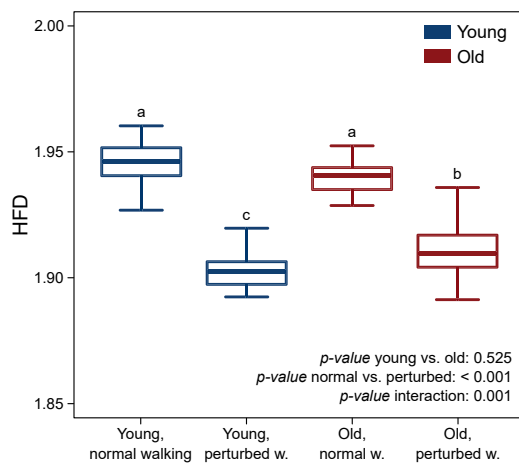
E1
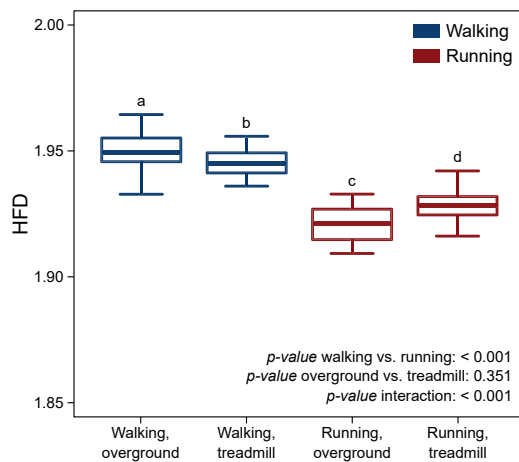
E2
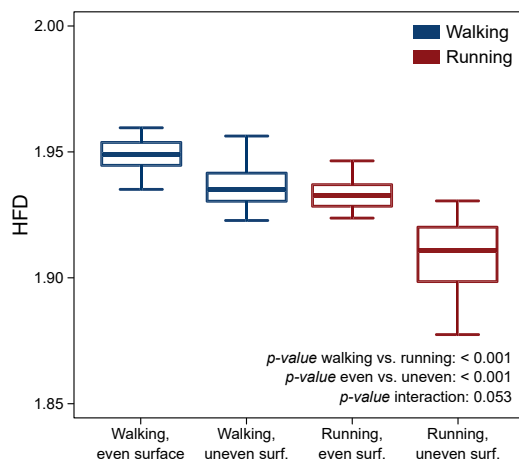
E3

Figure 4. Higuchi's Fractal Dimension of Motor Primitives

Boxplots describing the average Higuchi's fractal dimension (HFD) of motor primitives for the three experimental setups (E1, walking and running, overground and treadmill; E2, walking and running, even and uneven surface; E3, young and old, unperturbed and perturbed walking). Values sharing the same letter are not to be considered significantly different (results of the post-hoc analysis, where relevant).

scales, showing similar features independently on the spatial and temporal resolution we use to look at them (Higuchi, 1988; Kešić and Spasić, 2016; Smits et al., 2016; Theiler, 1990). The HFD of a monodimensional time series is a number between 1 and 2, with higher values denoting higher complexity of the signal (Smits et al., 2016). It has recently been shown that complexity in brain activity, measured by HFD, increases with maturation only to decline with aging and pathology (Kešić and Spasić, 2016; Smits et al., 2016; Zappasodi et al., 2014). Here, we show that the complexity of motor primitives is associated with external perturbations. Specifically, HFD decreases (i.e., complexity decreases) when locomotion is challenged by external perturbations in both young and older adults, even though older adults did not modulate complexity as much as the young during perturbed walking. In addition, we showed that running presented less complex motor primitives than walking, but treadmill and overground locomotion shared similar complexity values. Taken together, these results support the reduced sMLE values associated with perturbations, indicating the need for a simplification of motor control when locomotion is challenged.

In the past, we used the FWHM of motor primitives as a measure of motor control's robustness (Santuz et al., 2018a). Our conclusion was that wider (i.e., timewise longer active) primitives indicate more robust control (Santuz et al., 2018a). We reasoned that the overlap of chronologically adjacent synergies increased the fuzziness (Gentili, 2018; Meghdadi, 2004) of temporal boundaries allowing for easier shifts between one synergy (or gait phase) to the other (Santuz et al., 2018a), a conclusion that fits the optimal feedback control theory (Scott, 2004; Tuthill and Azim, 2018). For the CNS, this solution must come at a cost: the reduction of accuracy or, as others called it, optimality (Meghdadi, 2004) or efficiency (Pryluk et al., 2019). For instance, it has been recently found that human neurons allow less vocabulary overlap than monkey's, showing a trade-off between accuracy (complex human feature) and robustness (basic, typical of non-human primates) across species (Pryluk et al., 2019). In this study we confirmed a widening of motor primitives in those conditions that were more challenging than their equivalent baseline and in aging. Specifically, we considered running as a more challenging locomotion type than walking (Ekizos et al., 2018), treadmill as more challenging than overground locomotion (Dingwell and Cusumano, 2000), and perturbed locomotion as more challenging than unperturbed (Santuz et al., 2018a). We found an effect of external perturbations and aging on the widening of motor primitives.

However, we discovered that aging and the more challenging locomotion conditions not only imply wider primitives but also different local stability and complexity of neural control. We calculated lower sMLE (i.e., lower local instability) and lower HFD (i.e., lower complexity) in running compared with walking and in perturbed compared with unperturbed locomotion. Moreover, sMLE were lower in old compared with young adults. These outcomes indicate that the robustness of motor control is achieved not only by allowing motor primitives to be wider and fuzzier but also by making them less locally unstable and less complex. We recently found that the classical calculation of sMLE from kinematic data (e.g., by considering the trajectories of specific body landmarks recorded via motion capture) shows increased local instability in the presence of perturbations in both humans (Ekizos et al., 2018, 2017; Santuz et al., 2018a) and mice (Santuz et al., 2019). Our interpretation of this apparent discordance lies in the results of the present study. The sMLE calculation by means of state space reconstruction acts as a representation of the human locomotor system as a whole (Dingwell and Cusumano, 2000). Thus, increased positive sMLE mean higher sensitivity of the entire dynamical system to infinitesimal perturbations (Dingwell and Cusumano, 2000). The analysis we propose, though, aims to describe the CNS as a subsystem for the control of the main system's motion. This rationale tells us that the two descriptions are intrinsically different, possibly because they describe different portions of the "human being" as a dynamical system. From this perspective, it is not surprising that two different approaches give opposite results. In fact, the lower local instability and complexity of motor primitives might describe a strategy employed by the CNS to maintain acceptable levels of functionality when challenges are added globally to locomotion. The analysis of Lyapunov exponents has been used on EMG data as well (Kang and Dingwell, 2009). In that work, the authors found greater local dynamic instability in old compared with young adults. However, the authors only considered four muscles and made use of an eight-dimensional state space containing the four muscle activations and their time derivatives. These choices unfortunately made the work of Kang and Dingwell not directly comparable to ours.
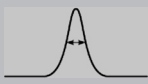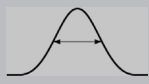
Experiment	Synergy			p Value
E1	Weight acceptance	Walking	Running	<0.001
	Propulsion	Walking	Running	<0.001
	Early swing	Walking	Running	0.013
	Late swing	–	–	–
E2	Weight acceptance	Walking	Running	<0.001
	Propulsion	Walking	Running	<0.001
	Early swing	Walking	Running	<0.001
		Unperturbed	Perturbed	0.005
	Late swing	Walking	Running	0.001
		Unperturbed	Perturbed	<0.001
E3	Weight acceptance	Young	Old	<0.001
		Unperturbed	Perturbed	0.037
	Propulsion	Young	Old	<0.001
	Early swing	Young	Old	<0.001
		Unperturbed	Perturbed	0.042
	Late swing	Young	Old	<0.001
		Unperturbed	Perturbed	0.002

Table 2. Widening of Motor Primitives
Summary of the conditions that had an effect on the full width at half maximum of the motor primitives extracted from the data of the three experimental setups (E1, walking and running, overground and treadmill; E2, walking and running, even and uneven surface; E3, young and old, unperturbed and perturbed walking). Motor primitives are the temporal coefficients of the four fundamental synergies for locomotion. Detailed boxplots are available in Figure S2.

In conclusion, our analysis of neuromotor dynamics reveals that fuzzier, less unstable, and less complex muscle activation patterns are generated by the CNS in the presence of challenging conditions to cope with perturbations (Santuz et al., 2018a). The instability and complexity of neural control decrease when movement is challenged, ensuring robust locomotion control across a variety of settings.

Limitations of the Study

We cannot exclude (and can in fact expect) that the human system is both deterministic and stochastic. This important observation implies that our outcomes, especially those concerning the sMLE, might be influenced by both the deterministic properties of the system as well as the dynamical and measurement noise (Kantz and Schreiber, 2004). Moreover, the interpretation of the word "stability" itself can be a source of controversy, for instance, if no difference is made between *local* and *orbital* or even *global* stability (Dingwell and Hyun, 2007). In fact, when Lyapunov exponents are used together with other approaches, such as that of the maximum Floquet multipliers, the outcomes can not only be different but also opposite, for instance, with one method indicating local instability and the other indicating orbital stability (Dingwell and Hyun, 2007). To reduce these and other similar inconsistencies, we believe that future scientific endeavors should focus on finding the biological nature of metrics like the sMLE, rather than remain on the descriptive and/or speculative side.

METHODS

All methods can be found in the accompanying Transparent Methods supplemental file.

REFERENCES

Ali, F., and Menzinger, M. (1999). On the local stability of limit cycles. Chaos 9, 348–356.

Aoi, S., Ohashi, T., Bamba, R., Fujiki, S., Tamura, D., Funato, T., Senda, K., Ivanenko, Y.P., and Tsuchiya, K. (2019). Neuromusculoskeletal model that walks and runs across a speed range with a few motor control parameter changes based on the muscle synergy hypothesis. Sci. Rep. 9, 369.

Bernstein, N.A. (1967). The Co-ordination and Regulation of Movements (Pergamon Press).

Bizzi, E., Cheung, V.C.-K., D'Avella, A., Saltiel, P., and Tresch, M.C. (2008). Combining modules for movement. Brain Res. Rev. 57, 125–133.

Bizzi, E., Mussa-Ivaldi, F.A., and Giszter, S.F. (1991). Computations underlying the execution of movement: a biological perspective. Science 253, 287–291.

Bradley, E., and Kantz, H. (2015). Nonlinear time-series analysis revisited. Chaos 25, 097610.

Cappellini, G., Ivanenko, Y.P., Martino, G., MacLellan, M.J., Sacco, A., Morelli, D., and Lacquaniti, F. (2016). Immature spinal locomotor output in children with cerebral palsy. Front. Physiol. 7, 1–21.

Cappellini, G., Ivanenko, Y.P., Poppele, R.E., and Lacquaniti, F. (2006). Motor patterns in human walking and running. J. Neurophysiol. 95, 3426–3437.

Daley, M.A. (2016). Non-steady locomotion. In Understanding Mammalian Locomotion (John Wiley & Sons, Inc), pp. 277–306.

Dingwell, J.B., and Cusumano, J.P. (2000). Nonlinear time series analysis of normal and pathological human walking. Chaos 10, 848–863.

Dingwell, J.B., and Hyun, G.K. (2007). Differences between local and orbital dynamic stability during human walking. J. Biomech. Eng. 129, 586–593.

Ekizos, A., Santuz, A., and Arampatzis, A. (2017). Transition from shod to barefoot alters dynamic stability during running. Gait Posture 56, 31–36.

Ekizos, A., Santuz, A., Schroll, A., and Arampatzis, A. (2018). The maximum lyapunov exponent during walking and running: reliability assessment of different marker-sets. Front. Physiol. 9, 1101.

Faisal, A.A., Selen, L.P.J., and Wolpert, D.M. (2008). Noise in the nervous system. Nat. Rev. Neurosci. 9, 292–303.

Gentili, P.L. (2018). The fuzziness of the molecular world and its perspectives. Molecules 23, E2074.

Giszter, S.F. (2015). Motor primitives-new data and future questions. Curr. Opin. Neurobiol. 33, 156–165.

Harris, C.M., and Wolpert, D.M. (1998). Signal-dependent noise determines motor planning. Nature 394, 780–784.

Higuchi, T. (1988). Approach to an irregular time series on the basis of the fractal theory. Phys. D Nonlinear Phenom. 31, 277–283.

Ivanenko, Y.P., Poppele, R.E., and Lacquaniti, F. (2004). Five basic muscle activation patterns account for muscle activity during human locomotion. J. Physiol. 556, 267–282.

Kang, H.G., and Dingwell, J.B. (2009). Dynamics and stability of muscle activations during walking in healthy young and older adults. J. Biomech. 42, 2231–2237.

Kantz, H., and Schreiber, T. (2004). Nonlinear Time Series Analysis, Second Edition (Cambridge University Press).

Kesić, S., and Spasić, S.Z. (2016). Application of Higuchi's fractal dimension from basic to clinical neurophysiology: a review. Comput. Methods Programs Biomed. 133, 55–70.

Kibushi, B., Moritani, T., and Kouzaki, M. (2018). Local dynamic stability in temporal pattern of intersegmental coordination during various stride time and stride length combinations. Exp. Brain Res. 237, 257–271.

Kitano, H. (2004). Biological robustness. Nat. Rev. Genet. 5, 826–837.

Lacquaniti, F., Ivanenko, Y.P., and Zago, M. (2012). Patterned control of human locomotion. J. Physiol. 590, 2189–2199.

Lorenz, E.N. (1963). Deterministic nonperiodic flow. J. Atmos. Sci. 20, 130–141.

Martino, G., Ivanenko, Y.P., D'Avella, A., Serrao, M., Ranavolo, A., Draicchio, F., Cappellini, G., Casali, C., and Lacquaniti, F. (2015). Neuromuscular adjustments of gait associated with unstable conditions. J. Neurophysiol. 114, 2867–2882.

Martino, G., Ivanenko, Y.P., Serrao, M., Ranavolo, A., D'Avella, A., Draicchio, F., Conte, C., Casali, C., and Lacquaniti, F. (2014). Locomotor patterns in cerebellar ataxia. J. Neurophysiol. *112*, 2810–2821.

Meghdadi, A.H. (2004). On Robustness of Evolutionary Fuzzy Control Systems, in: IEEE Annual Meeting of the Fuzzy Information, 2004. Processing NAFIPS '04, *Vol. 1* (IEEE), pp. 254–258, https://doi.org/10.1109/NAFIPS.2004.1336287.

Monaco, V., Ghionzoli, A., and Micera, S. (2010). Age-related modifications of muscle synergies and spinal cord activity during locomotion. J. Neurophysiol. *104*, 2092–2102.

Nutt, J.G., Marsden, C.D., and Thompson, P.D. (1993). Human walking and higher-level gait disorders, particularly in the elderly. Neurology *43*, 268.

Packard, N.H., Crutchfield, J.P., Farmer, J.D., and Shaw, R.S. (1980). Geometry from a time series. Phys. Rev. Lett. *45*, 712–716.

Pryluk, R., Kfir, Y., Gelbard-Sagiv, H., Fried, I., and Paz, R. (2019). A tradeoff in the neural code across regions and species. Cell *23*, 22–27.

Rabinovich, M., and Abarbanel, H.D. (1998). The role of chaos in neural systems. Neuroscience *87*, 5–14.

Rosenstein, M.T., Collins, J.J., and De Luca, C.J. (1993). A practical method for calculating largest Lyapunov exponents from small data sets. Phys. D *65*, 117–134.

Santuz, A., Akay, T., Mayer, W.P., Wells, T.L., Schroll, A., and Arampatzis, A. (2019). Modular organization of murine locomotor pattern in the presence and absence of sensory feedback from muscle spindles. J. Physiol. *597*, 3147–3165.

Santuz, A., Ekizos, A., Eckardt, N., Kibele, A., and Arampatzis, A. (2018a). Challenging human locomotion: stability and modular organisation in unsteady conditions. Sci. Rep. *8*, 2740.

Santuz, A., Ekizos, A., Janshen, L., Baltzopoulos, V., and Arampatzis, A. (2017a). On the methodological implications of extracting muscle synergies from human locomotion. Int. J. Neural Syst. *27*, 1750007.

Santuz, A., Ekizos, A., Janshen, L., Baltzopoulos, V., and Arampatzis, A. (2017b). The influence of footwear on the modular organization of running. Front. Physiol. *8*, 958.

Santuz, A., Ekizos, A., Janshen, L., Mersmann, F., Bohm, S., Baltzopoulos, V., and Arampatzis, A. (2018b). Modular control of human movement during running: an open access data set. Front. Physiol. *9*, 1509.

Scott, S.H. (2004). Optimal feedback control and the neural basis of volitional motor control. Nat. Rev. Neurosci. *5*, 532–545.

Shinar, G., and Feinberg, M. (2010). Structural sources of robustness in biochemical reaction networks. Science *327*, 1389–1391.

Smits, F.M., Porcaro, C., Cottone, C., Cancelli, A., Rossini, P.M., and Tecchio, F. (2016). Electroencephalographic fractal dimension in healthy ageing and Alzheimer's disease. PLoS One *11*, e0149587.

Theiler, J. (1990). Estimating the fractal dimension of chaotic time series. Lincoln Lab. J. *3*, 63–86.

Ting, L.H., Chiel, H.J., Trumbower, R.D., Allen, J.L., McKay, J.L., Hackney, M.E., and Kesar, T.M. (2015). Neuromechanical principles underlying movement modularity and their implications for rehabilitation. Neuron *86*, 38–54.

Tresch, M.C., Saltiel, P., and Bizzi, E. (1999). The construction of movement by the spinal cord. Nat. Neurosci. *2*, 162–167.

Tuthill, J.C., and Azim, E. (2018). Proprioception. Curr. Biol. *28*, R194–R203.

Wisse, M., Schwab, A.L., van der Linde, R.Q., and van der Helm, F.C.T. (2005). How to keep from falling forward: Elementary swing leg action for passive dynamic walkers. IEEE Trans. Robot. *21*, 393–401.

Zappasodi, F., Olejarczyk, E., Marzetti, L., Assenza, G., Pizzella, V., and Tecchio, F. (2014). Fractal dimension of EEG activity senses neuronal impairment in acute stroke. PLoS One *9*, e100199.

Supplemental Information

Neuromotor Dynamics of Human

Locomotion in Challenging Settings

Alessandro Santuz, Leon Brüll, Antonis Ekizos, Arno Schroll, Nils Eckardt, Armin Kibele, Michael Schwenk, and Adamantios Arampatzis

Neuromotor dynamics of human locomotion in challenging settings

Supplemental Information file

Transparent Methods (part of the Supplemental Information)

This study was reviewed and approved by the Ethics Committees of the Humboldt-Universität zu Berlin, Kassel University and Heidelberg University. All the participants gave written informed consent for the experimental procedure, in accordance with the Declaration of Helsinki.

Experimental protocols

For the three experimental protocols we recruited 86 healthy volunteers and divided them into four groups. The first group of 30 (henceforth G1, 15 males and 15 females, height 173 ± 10 cm, body mass 68 ± 12 kg, age 27 ± 5 years, means $\pm$ standard deviation) was assigned to the first experimental protocol (E1). The second group of 18 (G2, 11 males and 7 females, height 176 ± 7 cm, body mass 71 ± 13 kg, age 24 ± 3 years) was assigned to the second experimental protocol (E2). The last two groups where assigned to the third and last protocol (E3): one group of young (G3, 7 males and 12 females, height 171 ± 6 cm, body mass 65 ± 9 kg, age 27 ± 3 years) and one of older adults (G4, 5 males and 14 females, height 169 ± 8 cm, body mass 71 ± 12 kg, age 72 ± 6 years). All the participants completed a self-selected warm-up running on a treadmill, typically lasting between 3 and 5 min (Santuz et al., 2018b, 2016). After being instructed about the protocol, they completed a different set of measurements, depending on the protocol they were assigned to.

The experimental protocol E1 consisted of walking (at 1.40 m/s) and running (at 2.80 m/s) overground and on a treadmill (mercury, H-p-cosmos Sports & Medical GmbH, Nussdorf,

Germany). The speeds were chosen as the commonly reported average comfortable locomotion

speeds (Santuz et al., 2016, 2017a). For the overground trials, we used a light-barrier system to

control the speeds (average values of 1.40 ± 0.03 and 2.80 ± 0.04 m/s) in two consecutive sectors

of 3 m each.

5   The experimental protocol E2 consisted of walking (1.10 m/s for females, 1.20 m/s for males)

and running (2.00 m/s for females, 2.20 m/s for males) on one standard (Laufergotest, Erich

Jäger, Würzburg, Germany) and one uneven-surface (Woodway®, Weil am Rhein, Germany,

Fig. S1, Movie S1) treadmill (Santuz et al., 2018a). The uneven-surface treadmill's belt consisted

of terrasensa® classic modules (Sensa® by Huebner, Kassel, Germany). The speeds were chosen

10   after a pilot study in which we estimated the average comfortable locomotion speed on the

uneven-surface treadmill for males and females separately. Part of the data from this

experimental protocol was previously reported (Santuz et al., 2018a).

The experimental protocol E3 consisted of walking (1.20 m/s for the group of young adults G3,

1.10 m/s for the group of old adults G4) on a treadmill (BalanceTutor™, MediTouch LTD,

15   Netanya, Israel, Movie S1) that could provide mediolateral (through sudden displacement of the

belt-supporting platform) and anteroposterior (through rapid acceleration of the belt)

perturbations. The speeds were chosen after a pilot study in which we estimated the average

comfortable walking speed under perturbed conditions for young and old adults separately. Both

the perturbed and unperturbed trials lasted six minutes. The perturbed trials began with ~15 s of

20   unperturbed locomotion. Afterwards, the participants were informed about the beginning of

perturbations, which were delivered randomly (left or right mediolateral displacement or

acceleration) every ~3 s (G3: 3.786 ± 0.986 s; G4: 3.072 ± 0.434 sec) at unspecified phases of

the gait cycle. The interval between perturbations was a function of perturbation intensity (e.g.

the larger the displacement of the platform, the longer the time needed to reset the controls and start a new perturbation). Perturbation intensities were set in the proprietary software on a scale from 1 to 30. Mediolateral perturbations were set at an intensity of 15 for G3 and 10 for G4, while the accelerations were set at 12 for G3 and 8 for G4. Intensities were chosen after a pilot study in which we defined the "most challenging intensity before failure" for young and old adults separately.

The protocols E2 and E3 both included external perturbations to locomotion. However, the timing (continuous in E2 and every 3 s in E3) and mechanics (uneven surface in E2 and displacement of the treadmill's belt in E3) where of different nature. We chose two perturbation paradigms to allow for generalization of the outcomes. During the trials, the participants of both E2 and E3 were instructed to keep looking at a fixed spot in front of them and avoid looking at the treadmill's belt.

<u>EMG recordings</u>

Independently on the experimental protocol, the muscle activity of the following 13 ipsilateral (right side) muscles was recorded: gluteus medius (ME), gluteus maximus (MA), tensor fasciæ latæ (FL), rectus femoris (RF), vastus medialis (VM), vastus lateralis (VL), semitendinosus (ST), biceps femoris (long head, BF), tibialis anterior (TA), peroneus longus (PL), gastrocnemius medialis (GM), gastrocnemius lateralis (GL) and soleus (SO). The electrodes were positioned as extensively reported previously (Santuz et al., 2019, 2018b). After around 60 s habituation (Santuz et al., 2018a), we recorded two trials of 60 s for each participant with an acquisition frequency of 1 kHz (E2) or 2 kHz (E1 and E3) by means of a 16-channel wireless bipolar EMG system (E2: myon m320, myon AG, Schwarzenberg, Switzerland; E1 and E3: aktos, myolution GmbH, Ratingen, Germany). For the EMG recordings, we used foam-hydrogel electrodes with

snap connector (H124SG, Medtronic plc, Dublin, Ireland). The first 30 gait cycles of the recorded trial were considered for subsequent analysis (Santuz et al., 2018b). For the overground locomotion part of E1, due to limited length of the walkway (20 m), the participants were asked to repeat the trials 10 times for the subsequent concatenation of the data. Trials that did not

5   match the target speed with a tolerance of ± 0.05 m/s in walking and ± 0.10 m/s in running were repeated. For our analysis, we used all the available trials, taking the average of the interesting parameter when more than one trials were available. All the recordings can be downloaded from the supplementary data set, which is accessible at Zenodo (DOI: 10.5281/zenodo.2669485).

Gait cycle breakdown

10   The gait cycle breakdown was obtained by the elaboration of the data acquired by a 3D accelerometer operating at 148 Hz and synchronized with the EMG system. The accelerometer was strapped to the right shoe, over the most distal portion of the second to fourth metatarsal bones. The data was low-pass filtered using a 4th order IIR Butterworth zero-phase filter with cut-off frequency of 15 Hz. For estimating touchdown, we used the modified foot contact

15   algorithm developed by Maiwald and colleagues (Maiwald et al., 2009). For estimating lift-off, we adopted our foot acceleration and jerk algorithm (Santuz et al., 2018a). The jerk algorithm searches for the global maximum of the vertical acceleration between two consecutive touchdown events to estimate the lift-off (LOe, where the "e" stays for "estimated"). This estimation, however, does not provide an accurate identification of the lift-off and needs some

20   refinement. To get closer to the "real" lift-off timing, a characteristic minimum in the vertical acceleration (i.e. when the jerk equals zero) of the foot is identified in a reasonably small neighborhood of the LOe. We found [LOe – 250 ms, LOe + 100 ms] for both walking and running to be the sufficiently narrow interval needed to make the initial lift-off estimation.

However, we reduced this interval to [LOe – 150 ms, LOe + 100 ms] in the presence of external

perturbations (i.e. for E2 and E3). Both the approaches for the determination of touchdown and

lift-off have been validated using force plate data (AMTI BP600, Advanced Mechanical

Technology, Inc., Watertown, MA, USA) from 15 participants walking and running overground

5   at six different velocities without perturbations and from the data recorded in G1 overground.

We then calculated the true errors between the contact times detected via force plate and those

obtained from the acceleration data and used the averages to correct the calculations. Errors were

of 1.9 ms for touchdown and 13.1 ms for lift-off in walking and -4.1 ms and -13.2 ms for

running.

10   <u>Muscle</u> <u>synergies</u> <u>extraction</u>

For the experimental protocol E1, the overground EMG recordings were concatenated after

identification of the complete gait cycles (touchdown to touchdown of the right foot). For the

other protocols, we used the 30 gait cycles per trial described above. Muscle synergies data were

extracted through a custom script (R v3.6.1, R Found. for Stat. Comp.) using the classical

15   Gaussian non-negative matrix factorization (NMF) algorithm (Lee and Seung, 1999; Santuz et

al., 2017a, 2018a, 2018b). The raw EMG signals were band-pass filtered within the acquisition

device (cut-off frequencies 10 and 500 Hz). Then the signals were high-pass filtered, full-wave

rectified and lastly low-pass filtered using a 4th order IIR Butterworth zero-phase filter with cut-

off frequencies 50 Hz (high-pass) and 20 Hz (low-pass for creating the linear envelope of the

20   signal) as previously described (Santuz et al., 2018a). After subtracting the minimum, the

amplitude of the EMG recordings obtained from the single trials was normalized to the

maximum activation recorded for every individual muscle (i.e. every EMG channel was

normalized to its maximum in every trial) (Santuz et al., 2019, 2018b). Each gait cycle was then

time-normalized to 200 points, assigning 100 points to the stance and 100 points to the swing

phase (Santuz et al., 2019, 2018a, 2018b, 2017b). The reason for this choice is twofold (Santuz et

al., 2018b). First, dividing the gait cycle into two macro-phases helps the reader understanding

the temporal contribution of the different synergies, diversifying between stance and swing.

5 Second, normalizing the duration of stance and swing to the same number of points for all

participants (and for all the recorded gait cycles of each participant) makes the interpretation of

the results independent from the absolute duration of the gait events. Synergies were then

extracted through NMF as previously described (Santuz et al., 2018a, 2018b). For the analysis,

we considered the 13 muscles described above (ME, MA, FL, RF, VM, VL, ST, BF, TA, PL,

10 GM, GL and SO). The $m = 13$ time-dependent muscle activity vectors were grouped in a matrix

V with dimensions $m \times n$ (m rows and n columns). The dimension n represented the number of

normalized time points (i.e. 200*number of gait cycles). The matrix V was factorized using

NMF so that $V \approx V_R = WH$. The new matrix V_R, reconstructed multiplying the two matrices W

and H, approximates the original matrix V. The motor primitives (Dominici et al., 2011; Santuz

15 et al., 2017a) matrix H contained the time-dependent coefficients of the factorization with

dimensions $r \times n$, where the number of rows r represents the minimum number of synergies

necessary to satisfactorily reconstruct the original set of signals V. The motor modules (Gizzi et

al., 2011; Santuz et al., 2017a) matrix W, with dimensions $m \times r$, contained the time-invariant

muscle weightings, which describe the relative contribution of single muscles within a specific

20 synergy (a weight was assigned to each muscle for every synergy). H and W described the

synergies necessary to accomplish the required task (i.e. walking or swimming). The update rules

for W and H are presented in Equation (EQ1) and Equation (EQ2).

$$\begin{cases} H_{i+1} = H_i \dfrac{W_i^T V}{W_i^T W_i H_i} & \text{(EQ1)} \\[2ex] W_{i+1} = W_i \dfrac{V(H_{i+1})^T}{W_i H_{i+1}(H_{i+1})^T} & \text{(EQ2)} \end{cases}$$

The quality of reconstruction was assessed by measuring the coefficient of determination R^2 between the original and the reconstructed data (V and V_R, respectively). The limit of convergence for each synergy was reached when a change in the calculated R^2 was smaller than the 0.01% in the last 20 iterations (Santuz et al., 2017a) meaning that, with that amount of synergies, the signal could not be reconstructed any better. This operation was first completed by setting the number of synergies to 1. Then, it was repeated by increasing the number of synergies each time, until a maximum of 10 synergies. The number 10 was chosen to be lower than the number of muscles, since extracting a number of synergies equal to the number of measured EMG activities would not reduce the dimensionality of the data. Specifically, 10 is the rounded 75% of 13, which is the number of considered muscles (Santuz et al., 2019). For each synergy, the factorization was repeated 10 times, each time creating new randomized initial matrices W and H, in order to avoid local minima (D'Avella and Bizzi, 2005). The solution with the highest R^2 was then selected for each of the 10 synergies. To choose the minimum number of synergies required to represent the original signals, the curve of R^2 values versus synergies was fitted using a simple linear regression model, using all 10 synergies. The mean squared error (Cheung et al., 2005) between the curve and the linear interpolation was then calculated. Afterwards, the first point in the R^2-vs.-synergies curve was removed and the error between this new curve and its new linear interpolation was calculated. The operation was repeated until only two points were left on the curve or until the mean squared error fell below 10^{-4}. This was done to search for the

most linear part of the R^2-versus-synergies curve, assuming that in this section the reconstruction quality could not increase considerably when adding more synergies to the model.

Local dynamic stability of motor primitives

We assessed the local dynamic stability of motor primitives using the short-term maximum Lyapunov exponents (sMLE) (Rosenstein et al., 1993). Usually sMLE are extracted after reconstruction of the state space through delay-coordinate embedding starting from a measured one-dimensional time series (Packard et al., 1980). The state space is a set of all the possible states of a system at any given time, the variables of which might be position, velocity, temperature, color, species, voltage and many others (Lorenz, 1963; Packard et al., 1980; Rabinovich and Abarbanel, 1998). Yet, in our typical experimental setups involving complex living systems like humans, the state space is often unknown. Theoretically, the behavior of a purely chaotic dynamical system can be predicted by using only a small set of observations on its state (e.g. joint angles, or kinematics, or accelerations, etc.) without losing information on its properties (Ekizos et al., 2018; Santuz et al., 2018a). For this reason, it is common to use the recorded data to reconstruct the state space, usually by means of the "delay embedding theorem" (Takens, 1981). Typically sMLE are then calculated from data expanded in the state space (Lorenz, 1963; Packard et al., 1980). We avoided this passage by assuming that the space we are interested into had dimension equal to the factorization rank (i.e. the minimum number of synergies necessary to sufficiently reconstruct the original EMG signals). That is, the embedding dimension was determined by the NMF. The work from Sauer and colleagues (Sauer et al., 1991) allows to use n-dimensional measurements instead of the classical state space reconstruction. For instance, if one trial was factorized by NMF into four synergies, we would calculate the sMLE of the resulting four motor primitives using four as embedding dimension. This approach has the

advantage that it does not require the estimation of a suitable delay and embedding dimension, the latter being particularly sensitive to the presence of noise, which is very likely in experimental data (Dingwell et al., 2007). The motor primitives associated to the synergies extracted using the methods described above, were analyzed as follows. Each set of motor

5primitives was a time series of 30 gait cycles, normalized in time as described above (100 points for the stance and 100 for the swing, for a total of n=6000 points per trial). Primitives were then scaled to have the same variance by subtracting the mean and dividing by the standard deviation in order to avoid having different dynamical ranges across the data set (Kantz and Schreiber, 2004). For every point x_i in each time series (or set of motor primitives), we searched for the

10nearest neighbors of the point x_i excluding the neighborhood points $[x_{i-100}, x_{i+100}]$. This interval was chosen in order to impose a temporal separation between the nearest neighbors (Theiler window), making sure that they were on different trajectories (or gait cycles), as previously described (Rosenstein et al., 1993). Once the algorithm found the nearest neighbors, we proceeded to calculate the logarithm of the divergence between the trajectory of each point

15and its nearest neighbor's and for a maximum of 300 consecutive time points. For each trial, the divergence curve was calculated as the average of all divergence curves obtained from each point in the time series and their neighbors (Rosenstein et al., 1993). We then defined sMLE as the slope of the most linear part of the divergence curve, starting from the first point. To define linearity, we imposed the R^2 between the curve and its linear interpolation to be bigger than 0.9.

20Across all trials for each experimental setup, we then found the minimum number of points needed to reach a linear interpolation with $R^2 > 0.9$ and used these values to recalculate the final sMLE. The minimum number of points was three in E1, E2 and E3 and this is the value we used;

the maximum was 7 (E1), 8 (E2), and 6 (E3), with average values of 4.7 ± 0.9 (E1), 4.8 ± 1.0 (E2), 4.6 ± 0.6 (E3).

Higuchi's fractal dimension of motor primitives

To assess the irregularity (or complexity) of motor primitives, we calculated the Higuchi's fractal

5   dimension (HFD), assuming that these time series exhibit self-similarity properties (Higuchi, 1988; Kesić and Spasić, 2016; Smits et al., 2016; Theiler, 1990). Following the procedure first described by Higuchi (Higuchi, 1988), for each motor primitive $H(t)[H(1), H(2), ... H(n)]$, we constructed k sets of new time series, where k is an integer interval time and $2 < k < k_{max}$:

$$H_k^{t_0}: H(t_0), H(t_0 + k), H(t_0 + 2k), \dots, H\left[t_0 + int\left(\frac{n - t_0}{k}\right)k\right] \qquad (EQ3)$$

10   where t_0 is the first sample at initial time. The non-Euclidean length of each curve was defined as

$$L_{t_0}(k) = \frac{1}{k}\left\{ \frac{n-1}{int\left(\frac{n-t_0}{k}\right)k}\left[\sum_{i=1}^{int\left(\frac{n-t_0}{k}\right)k} |H(t_0 + ik) - H(t_0 + (i-1)k)| \right] \right\} \qquad (EQ4)$$

and for every considered k step the length of the motor primitive was defined as the average of the k sets of lengths as

$$L(k) = \frac{1}{k}\sum_{t_0=1}^{k} L_{t_0}(k) \qquad (EQ5).$$

15   If $L(k) \propto k^{-HFD}$, then the curve is fractal with dimension HFD and this should lead the plot of $\log(L(k))$ versus $\log(1/k)$ to fall on a straight line with slope -HFD. For each trial, the HFD of the primitives obtained by NMF were calculated separately and then averaged, so that each trial ultimately consisted of one HFD value. Since HFD increases with k_{max} until it reaches a plateau at $k_{plateau}$, we chose as k_{max} the average of the $k_{plateau}$ values obtained

20   from all trials. In this study, $k_{max} = 237$ time points.

Width of motor primitives

We compared motor primitives by evaluating the full width at half maximum (FWHM), a metric useful to describe the duration of activation patterns (Cappellini et al., 2006; Martino et al., 2014; Santuz et al., 2019, 2018a). The FWHM was calculated cycle-by-cycle as the number of points exceeding each cycle's half maximum, after subtracting the cycle's minimum and then averaged (Martino et al., 2014). The FWHM (and just this parameter) was calculated only for the motor primitives relative to fundamental synergies. A fundamental synergy can be defined as an activation pattern whose motor primitive shows a single main peak of activation (Santuz et al., 2018a). When two or more fundamental synergies are blended into one, a combined synergy appears. Combined synergies usually constitute, in our data, 10 to 30% of the total extracted synergies. Due to the lack of consent in the literature on how to interpret them, we excluded the combined synergies from the FWHM analysis. The recognition of fundamental synergies was carried out based on a previously reported approach (Santuz et al., 2017b, 2017a), which involves the creation of a training set and the subsequent supervised clustering of similar primitives.

Statistics

To investigate the main effects on the sMLE, HFD, and FWHM of locomotion type (i.e. walking or running), condition (i.e. overground or treadmill), perturbations and age, we fitted the data using a generalized linear model with Gaussian error distribution. The homogeneity of variances was tested using the Levene's test. If the residuals were normally distributed, we carried out a two-way repeated measures ANOVA with type II sum of squares, the independent variables being: locomotion type (walking or running) and condition (overground or treadmill) in E1; locomotion type (walking or running) and condition (perturbed or unperturbed) in E2;

locomotion condition (perturbed or unperturbed) and age (young or old) in E3. If the normality

assumptions on the residuals were not met, we used a robust (rank-based) ANOVA from the R

package Rfit (function "raov") (Kloke and McKean, 2012; McKean and Kloke, 2014). When an

interaction of the main effects was observed, we performed a least significant difference *post-hoc*

analysis with false discovery rate adjustment of the *p*-values. All the significance levels were set

to $\alpha = 0.05$ and the statistical analyses were conducted using R v3.6.1 (R Found. for Stat.

Comp.).

<u>Data and code</u> <u>availability</u>

In the supplementary data set accessible at Zenodo (DOI: 10.5281/zenodo.2669485) we made

available: a) the metadata with anonymized participant information, b) the raw EMG, c) the

touchdown and lift-off timings of the recorded limb, d) the filtered and time-normalized EMG, e)

the muscle synergies extracted via NMF and f) the code to process the data, including the scripts

to calculate the sMLE and HFD of motor primitives. In total, 476 trials from 86 participants are

included in the supplementary data set.

The file "participant_data.dat" is available in ASCII and RData (R Found. for Stat. Comp.)

format and contains:

- Code: the participant's code
- Experiment: the experimental setup in which the participant was involved (E1 =
  walking and running, overground and treadmill; E2 = walking and running, even-
  and uneven-surface; E3 = unperturbed and perturbed walking, young and old)
- Group: the group to which the participant was assigned (see methods for the details)
- Sex: the participant's sex (M or F)

- Speed: the speed at which the recordings were conducted in [m/s] (two values separated by a comma mean that recordings were done at two different speeds, i.e. walking and running)

- Age: the participant's age in years (participants were considered old if older than 65 years, but younger than 80)

- Height: the participant's height in [cm]

- Mass: the participant's body mass in [kg].

The files containing the gait cycle breakdown are available in RData (R Found. for Stat. Comp.) format, in the file named "CYCLE_TIMES.RData". The files are structured as data frames with 30 rows (one for each gait cycle) and two columns. The first column contains the touchdown incremental times in seconds. The second column contains the duration of each stance phase in seconds. Each trial is saved as an element of a single R list. Trials are named like "CYCLE_TIMES_P0020," where the characters "CYCLE_TIMES" indicate that the trial contains the gait cycle breakdown times and the characters "P0020" indicate the participant number (in this example the 20th). Please note that the overground trials of participants P0001 and P0009 and the second uneven-surface running trial of participant P0048 only contain 22, 27 and 23 cycles, respectively.

The files containing the raw, filtered and the normalized EMG data are available in RData (R Found. for Stat. Comp.) format, in the files named "RAW_EMG.RData" and "FILT_EMG.RData". The raw EMG files are structured as data frames with 30000 rows (one for each recorded data point) and 14 columns. The first column contains the incremental time in seconds. The remaining thirteen columns contain the raw EMG data, named with muscle abbreviations that follow those reported in the Materials and Methods section of this

Supplementary Materials file. Each trial is saved as an element of a single R list. Trials are

named like "RAW_EMG_P0053_OW_02", where the characters "RAW_EMG" indicate that the

trial contains raw EMG data, the characters "P0053" indicate the participant number (in this

example the 53rd), the characters "OW" indicate the locomotion type (E1: OW=overground

5 walking, OR=overground running, TW=treadmill walking, TR=treadmill running; E2:

EW=even-surface walking, ER=even-surface running, UW=uneven-surface walking,

UR=uneven-surface running; E3: NW=normal walking, PW=perturbed walking), and the

numbers "02" indicate the trial number (in this case the 2nd). The 10 trials per participant

recorded for each overground session (i.e. 10 for walking and 10 for running) were concatenated

10 into one. The filtered and time-normalized EMG data is named, following the same rules, like

"FILT_EMG_P0053_OW_02".

The files containing the muscle synergies extracted from the filtered and normalized EMG data

are available in RData (R Found. for Stat. Comp.) format, in the files named "SYNS_H.RData"

and "SYNS_W.RData". The muscle synergies files are divided in motor primitives and motor

15 modules and are presented as direct output of the factorization and not in any functional order.

Motor primitives are data frames with 6000 rows and a number of columns equal to the number

of synergies (which might differ from trial to trial) plus one. The rows contain the time-

dependent coefficients (motor primitives), one column for each synergy plus the time points

(columns are named e.g. "Time, Syn1, Syn2, Syn3", where "Syn" is the abbreviation for

20 "synergy"). Each gait cycle contains 200 data points, 100 for the stance and 100 for the swing

phase which, multiplied by the 30 recorded cycles, result in 6000 data points distributed in as

many rows. This output is transposed as compared to the one discussed in the methods section to

improve user readability. Each set of motor primitives is saved as an element of a single R list.

Trials are named like "SYNS_H_P0012_PW_02", where the characters "SYNS_H" indicate that

the trial contains motor primitive data, the characters "P0012" indicate the participant number (in

this example the 12th), the characters "PW" indicate the locomotion type (see above), and the

numbers "02" indicate the trial number (in this case the 2nd). Motor modules are data frames

5   with 13 rows (number of recorded muscles) and a number of columns equal to the number of

synergies (which might differ from trial to trial). The rows, named with muscle abbreviations

that follow those reported in the methods section, contain the time-independent coefficients

(motor modules), one for each synergy and for each muscle. Each set of motor modules relative

to one synergy is saved as an element of a single R list. Trials are named like

10   "SYNS_W_P0082_PW_02", where the characters "SYNS_W" indicate that the trial contains

motor module data, the characters "P0082" indicate the participant number (in this example the

82nd), the characters "PW" indicate the locomotion type (see above), and the numbers "02"

indicate the trial number (in this case the 2nd). Given the nature of the NMF algorithm for the

extraction of muscle synergies, the supplementary data set might show non-significant

15   differences as compared to the one used for obtaining the results of this paper.

The files containing the sMLE calculated from motor primitives are available in RData (R

Found. for Stat. Comp.) format, in the file named "sMLE.RData". sMLE results are presented in

a list of lists containing, for each trial, 1) the divergences, 2) the sMLE, and 3) the value of the

R^2 between the divergence curve and its linear interpolation made using the specified amount of

20   points. The divergences are presented as one-dimensional vectors. sMLE are one number like the

R^2 value. Trials are named like "sMLE_P0081_EW_01", where the characters "sMLE" indicate

that the trial contains sMLE data, the characters "P0081" indicate the participant number (in this

example the 81st), the characters "EW" indicate the locomotion type (see above), and the

numbers "01" indicate the trial number (in this case the 1st).

The files containing the HFD calculated from motor primitives are available in RData (R Found.

for Stat. Comp.) format, in the file named "HFD.RData". HFD results are presented in a list of

5   lists containing, for each trial, 1) the HFD, and 2) the interval time k used for the calculations.

HFDs are presented as one number, as are the interval times k. Trials are named like

"HFD_P0048_TR_01", where the characters "HFD" indicate that the trial contains HFD data,

the characters "P0048" indicate the participant number (in this example the 48th), the characters

"TR" indicate the locomotion type (see above), and the numbers "01" indicate the trial number

10   (in this case the 1st).

All the code used for the preprocessing of EMG data, the extraction of muscle synergies, the

calculation of sMLE and HFD is available in R (R Found. for Stat. Comp.) format. Explanatory

comments are profusely present throughout the scripts ("SYNS.R", which is the script to extract

synergies, "fun_NMF.R", which contains the NMF function, "sMLE.R", which is the script to

15   calculate the sMLE of motor primitives, "HFD.R", which is the script to calculate the HFD of

motor primitives, "fun_sMLE.R", which contains the sMLE function and "fun_HFD.R", which

contains the HFD function).

Fig. S1. Sketch of the uneven-surface treadmill used for the experimental protocol E2 described in the methods and related to Fig. 3 and Fig. 4. The belt of this treadmill was built to reproduce an uneven-terrain environment.
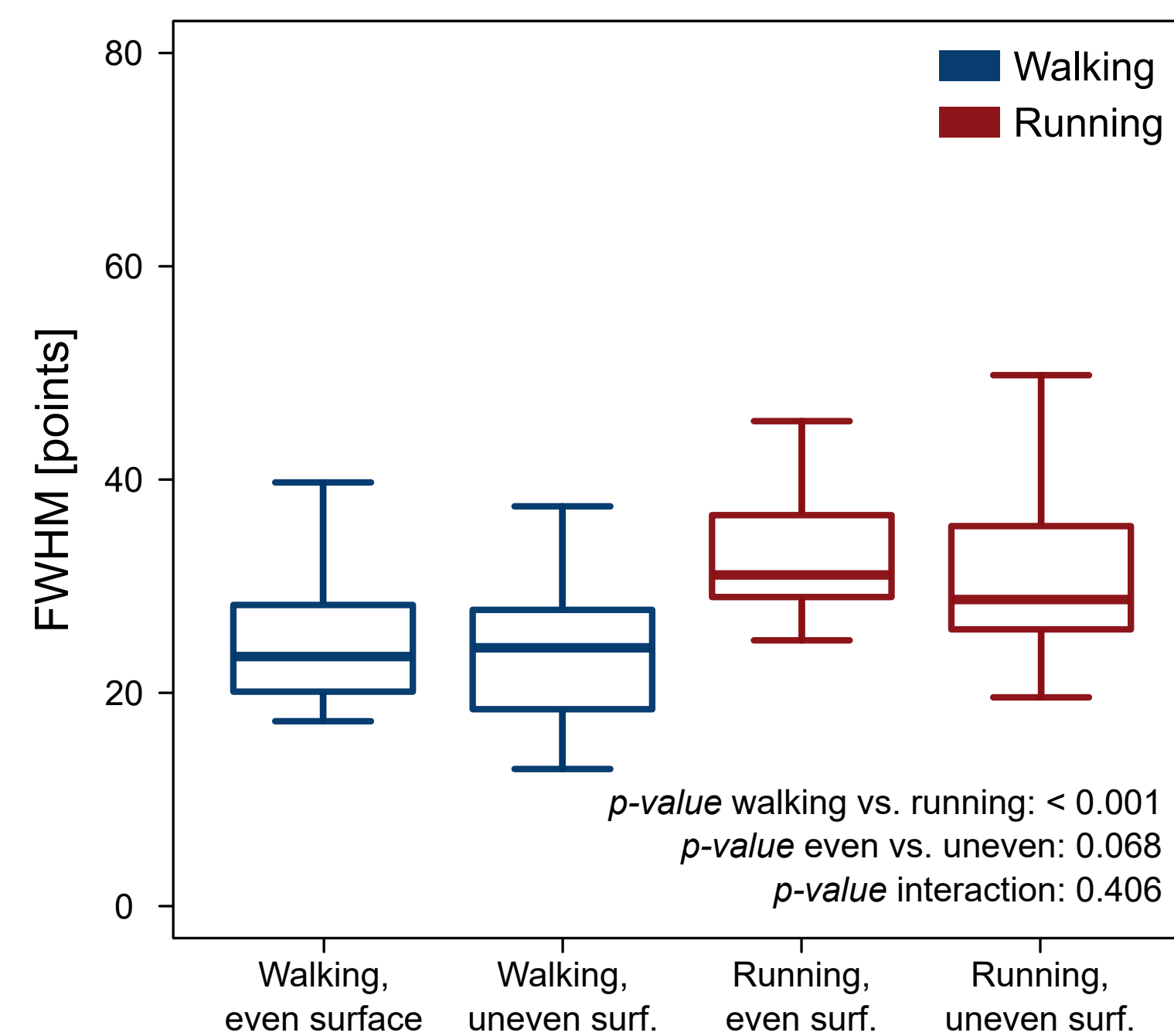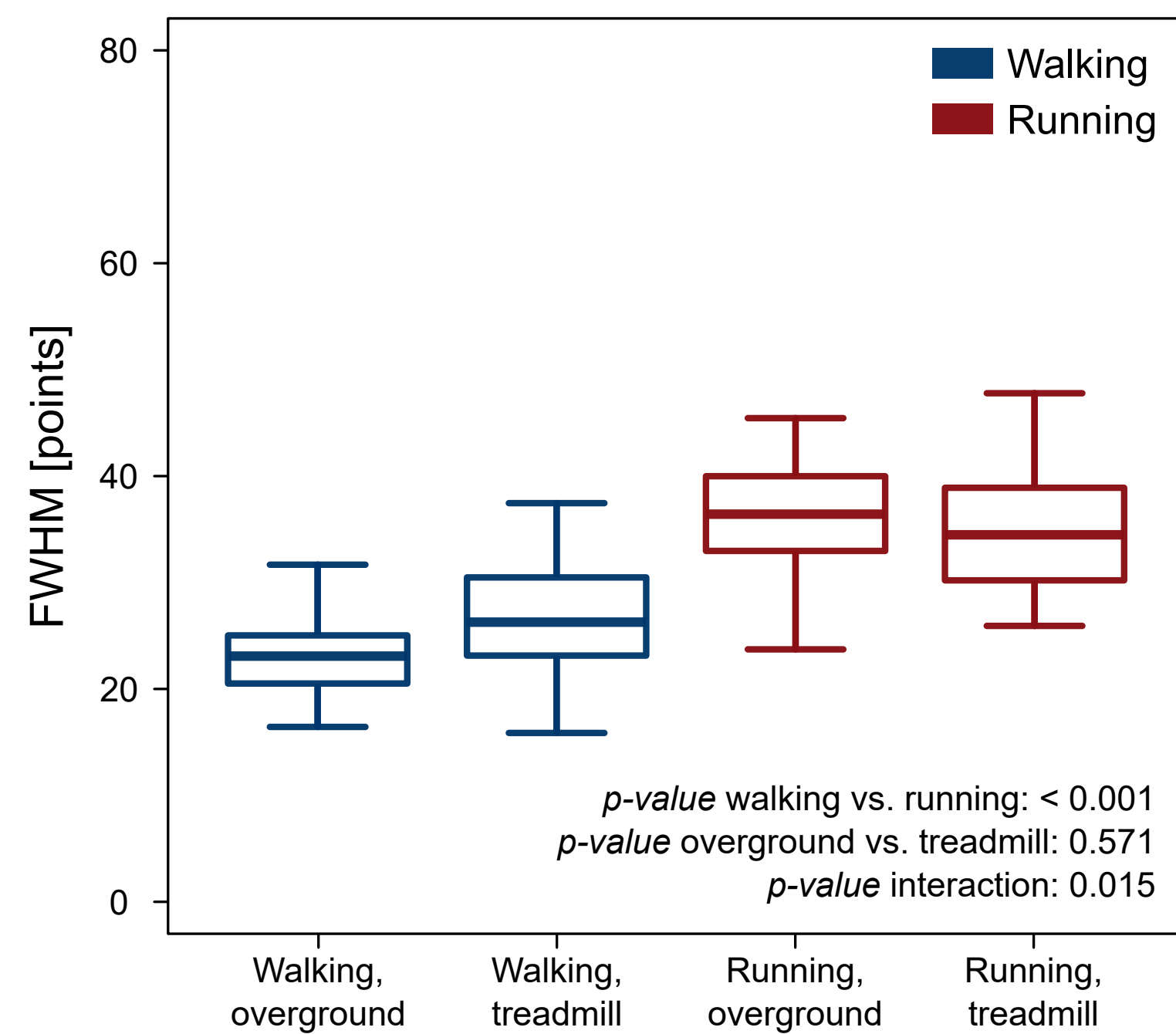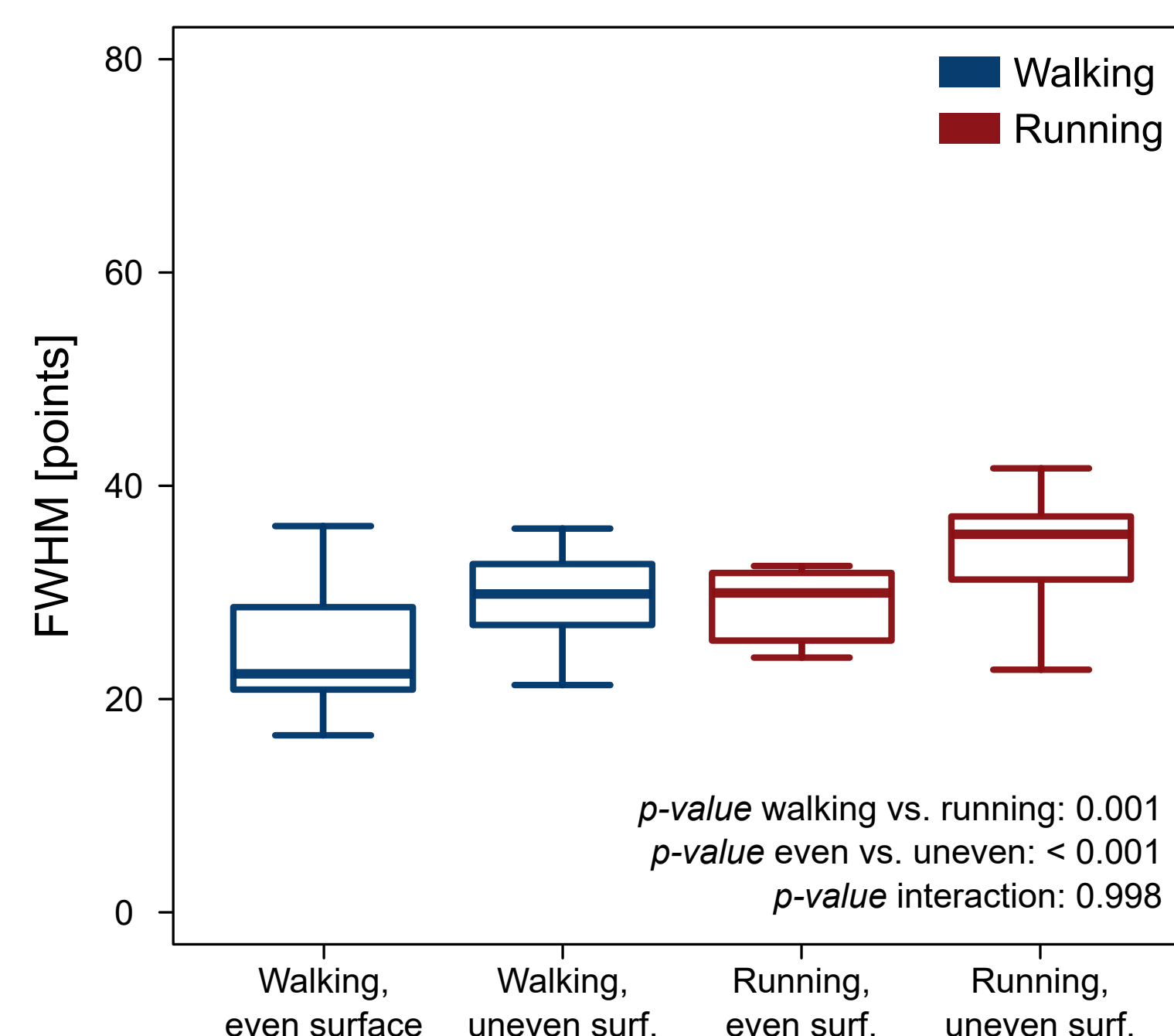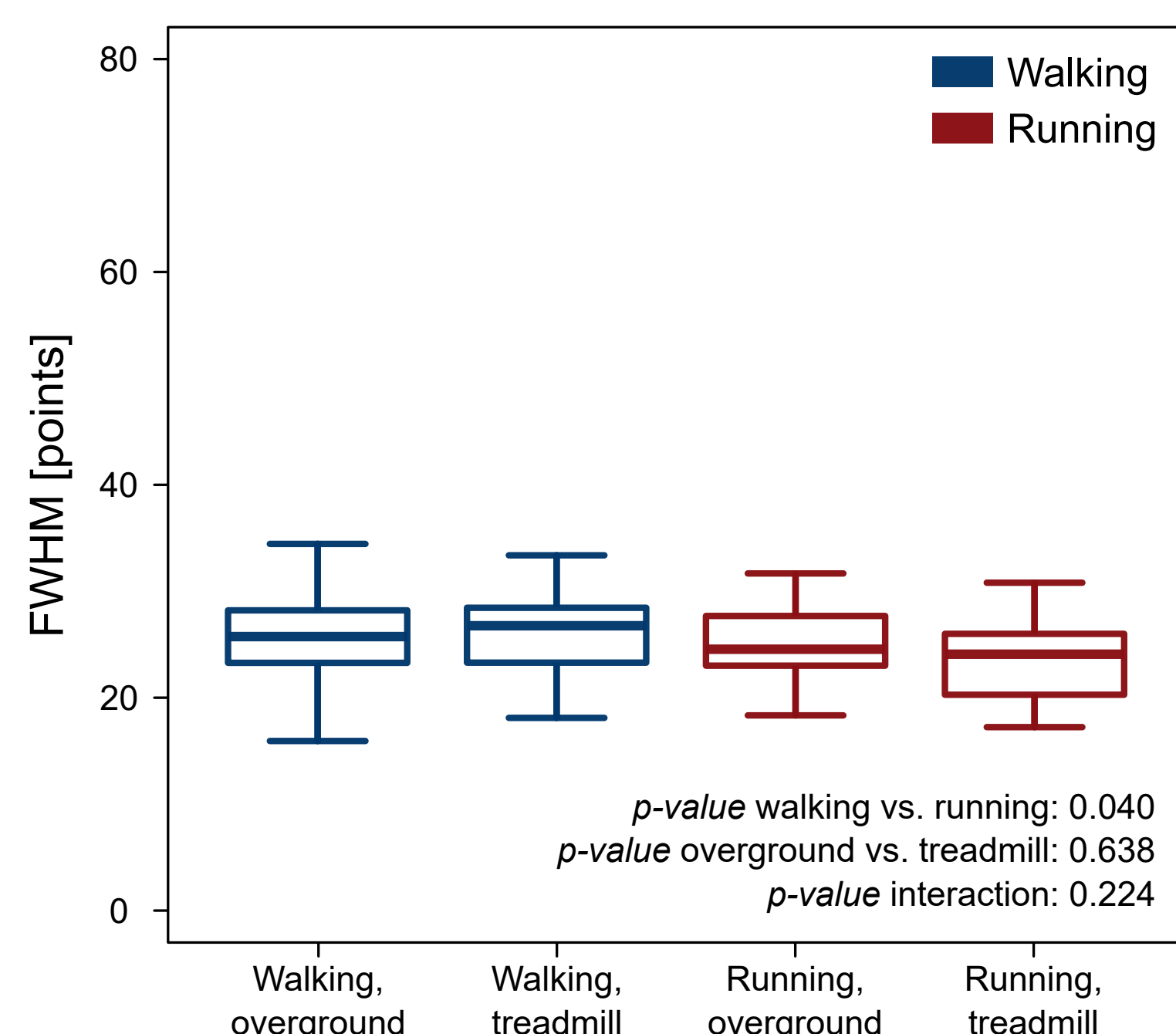
5
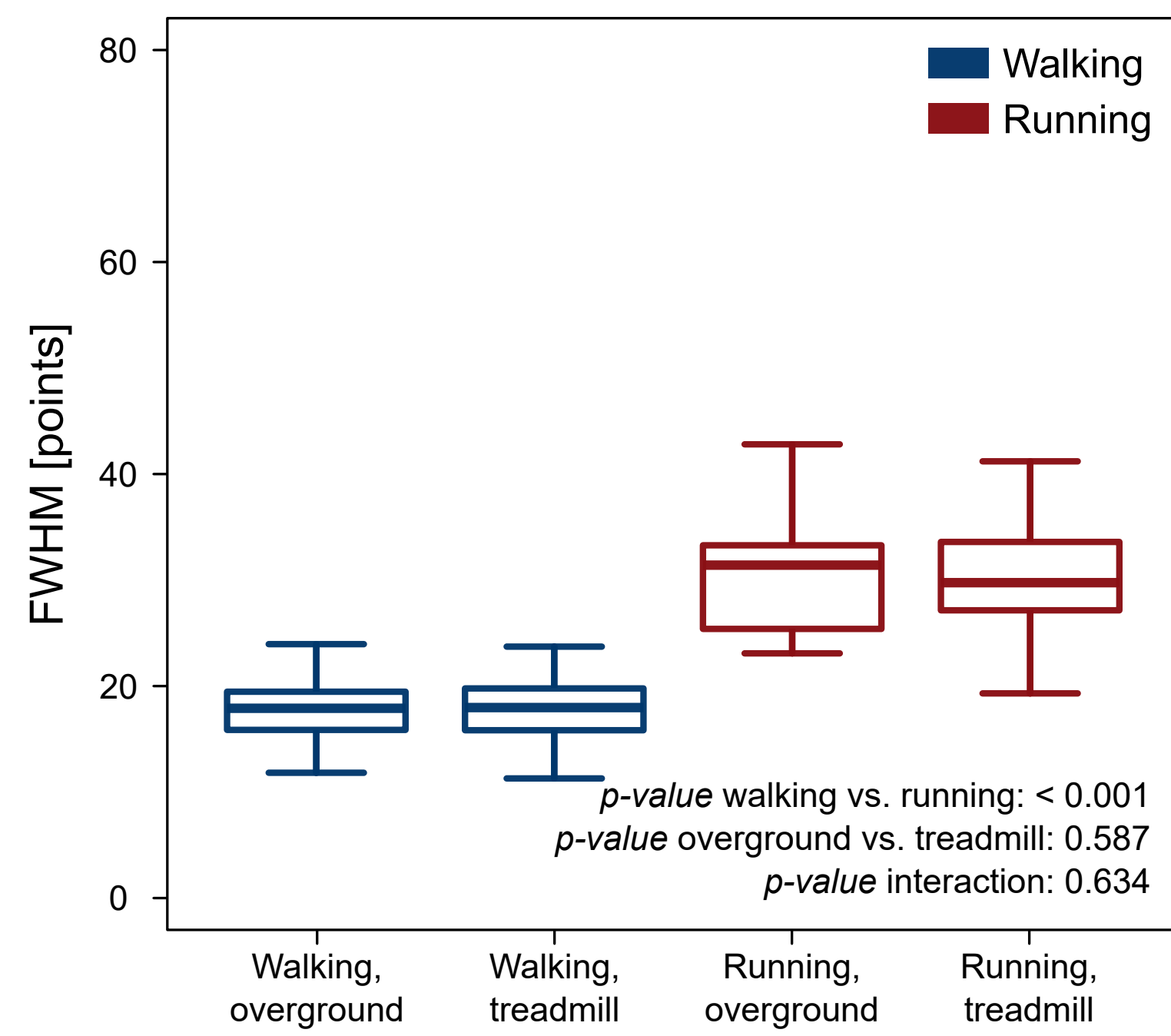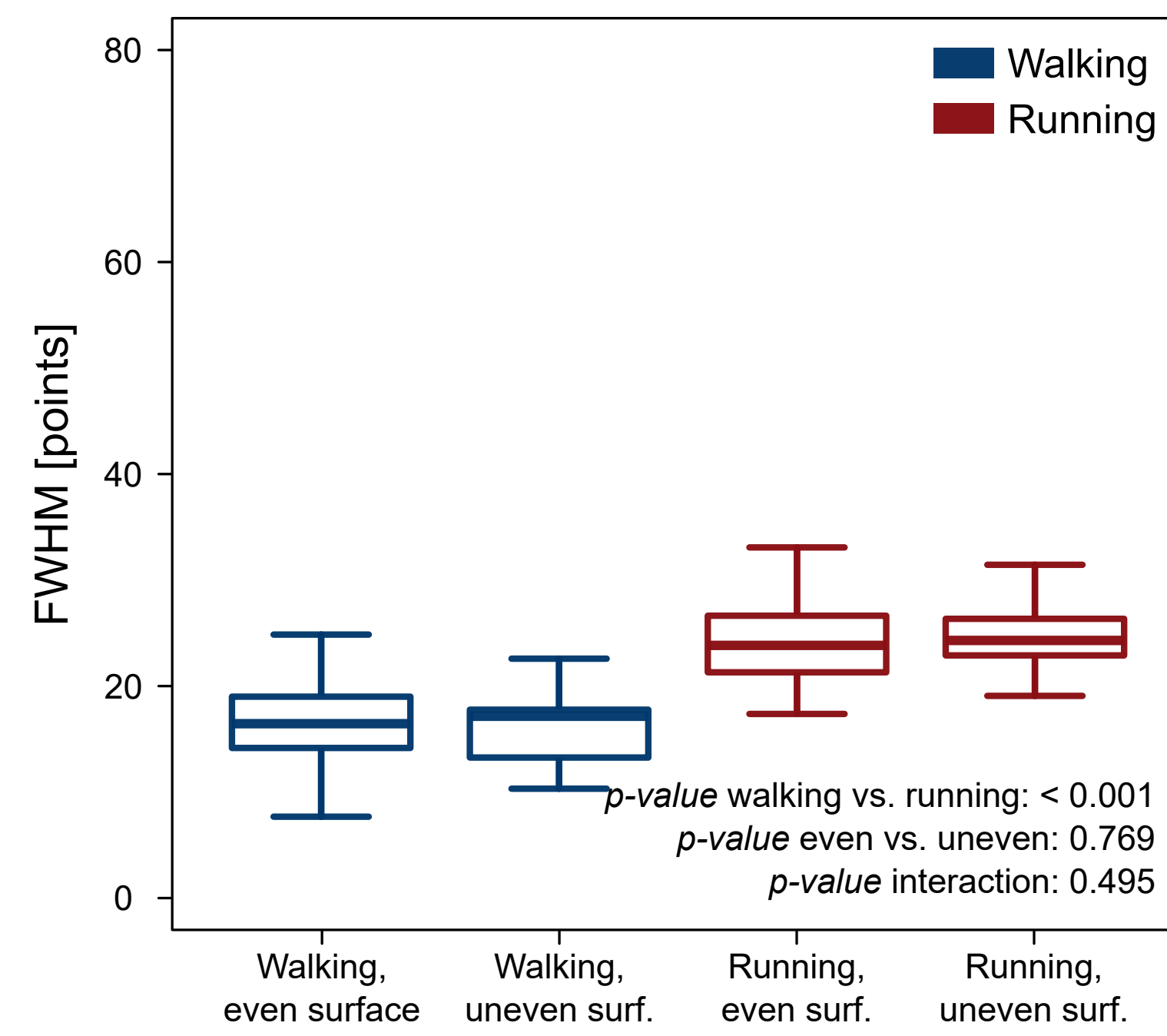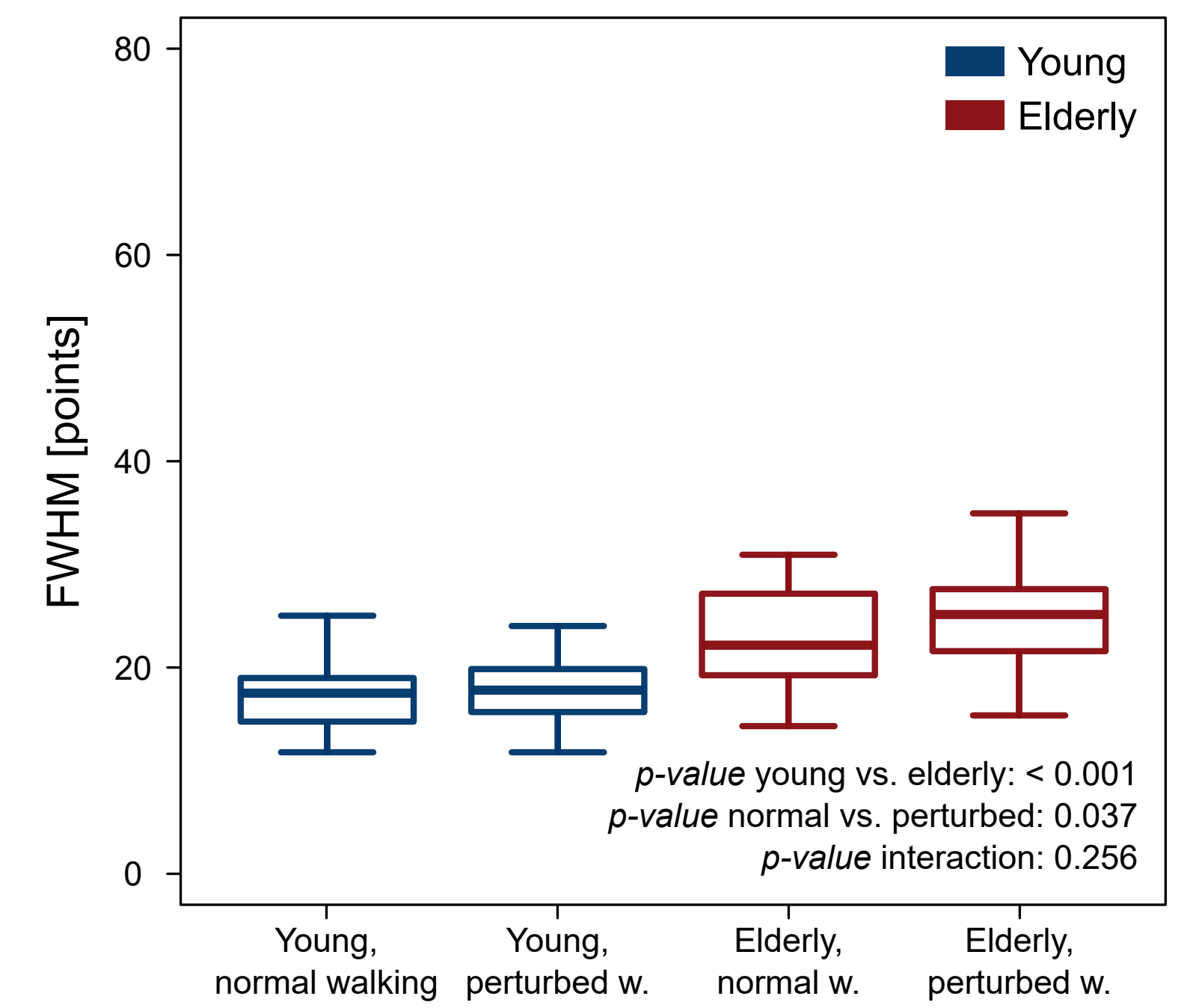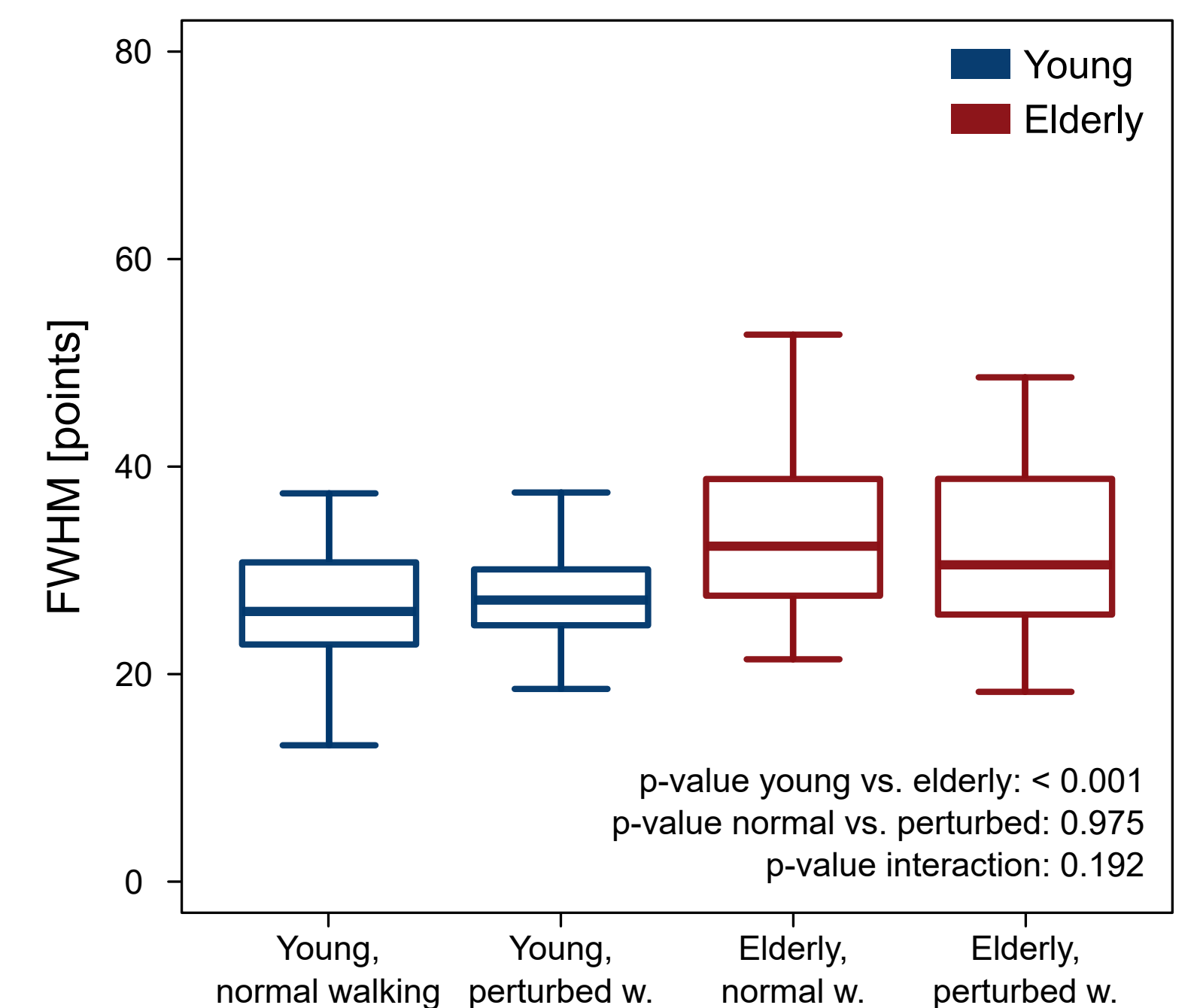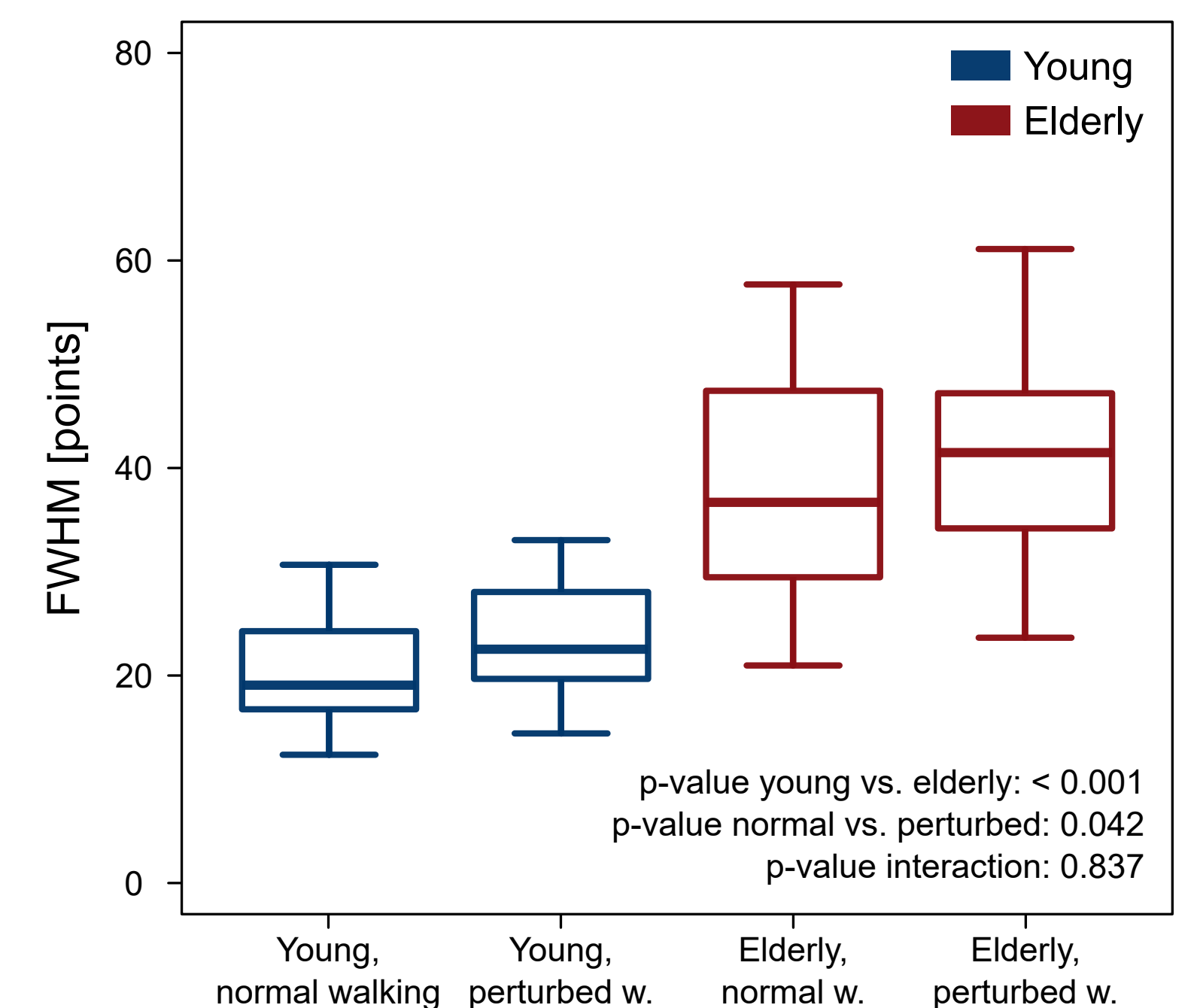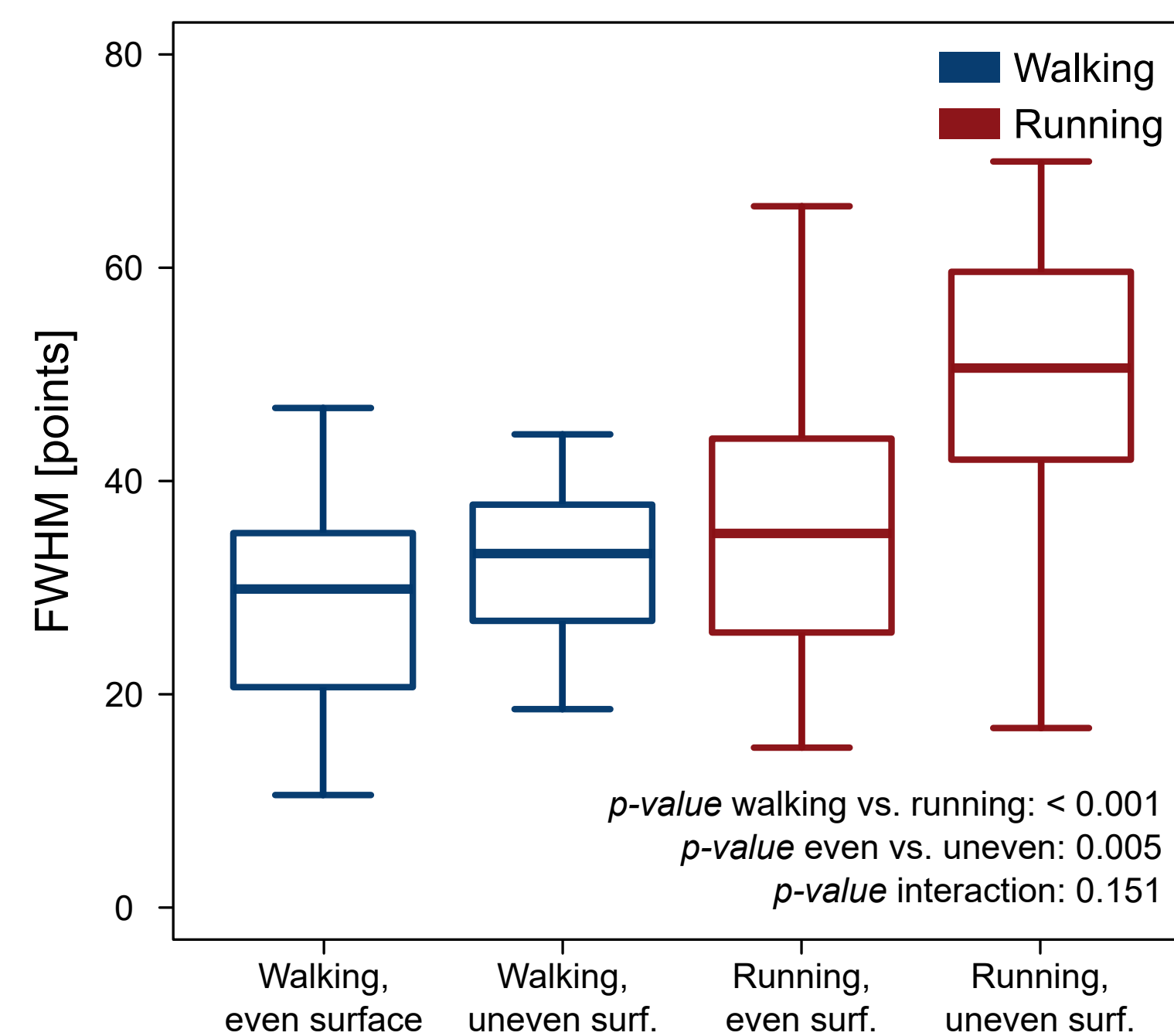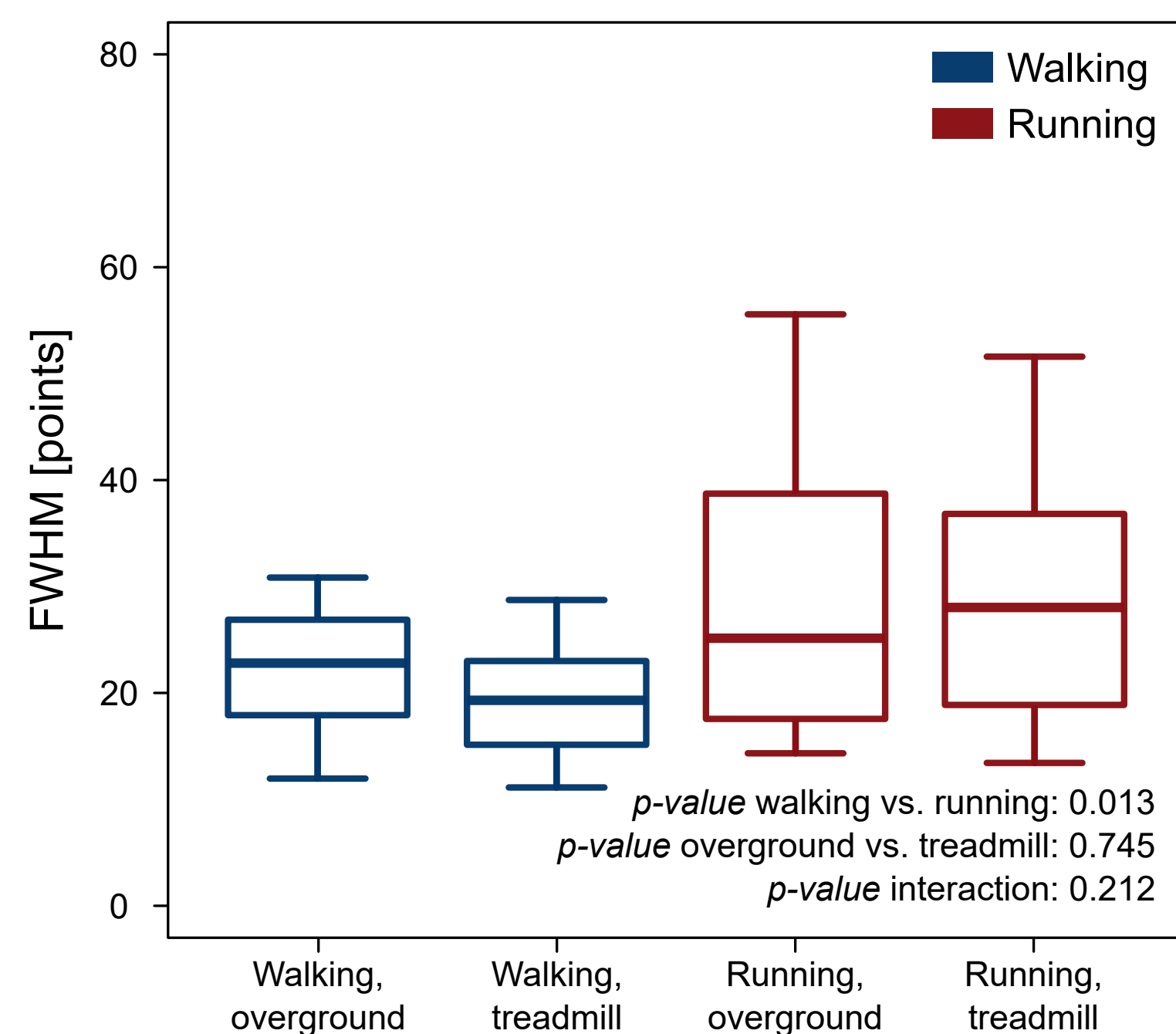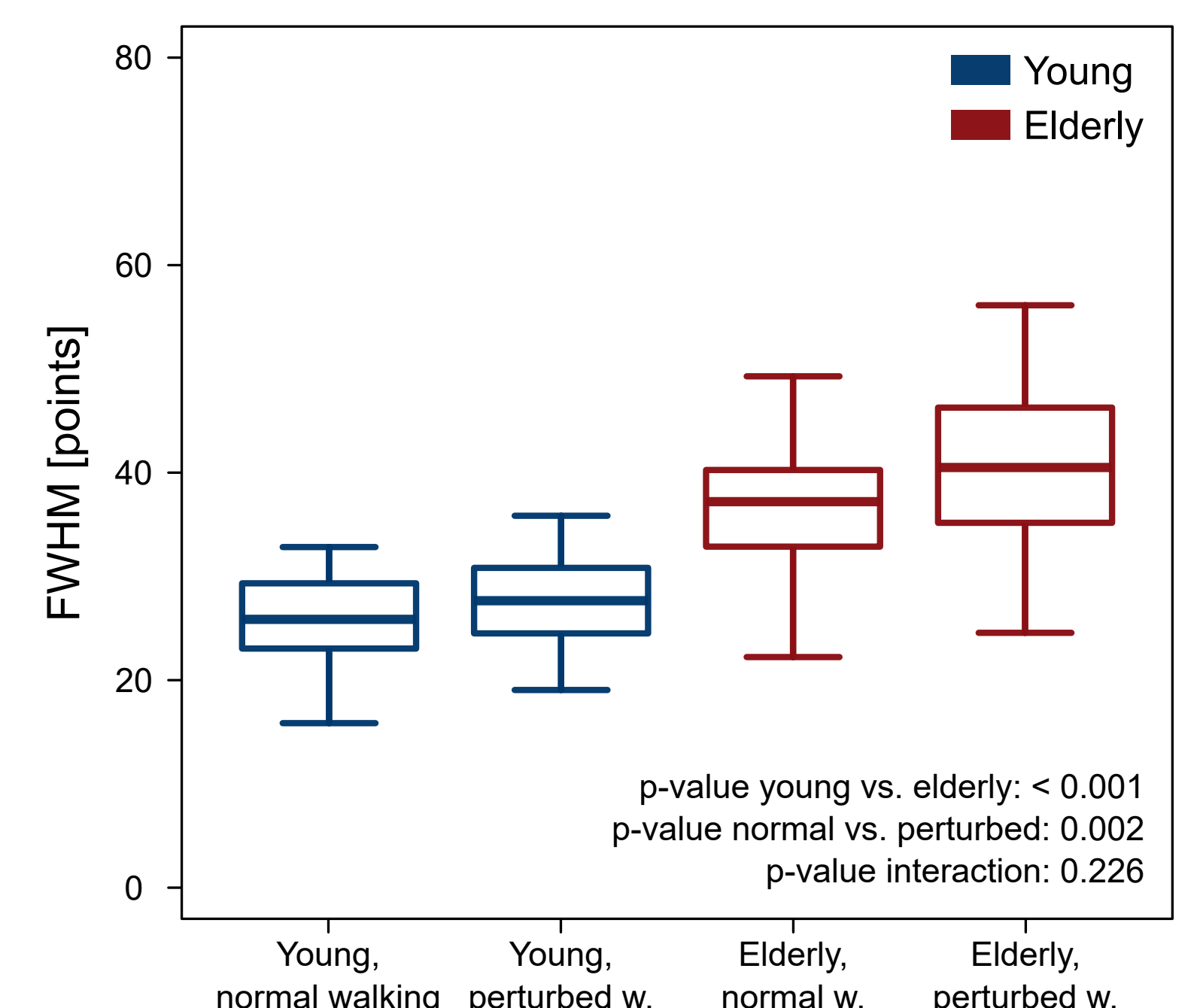
Fig. S2. Full width at half maximum of motor primitives related to Table 2. Boxplots

describing the full width at half maximum (FWHM) of the motor primitives extracted from the

data of the three experimental setups (E1 = walking and running, overground and treadmill; E2 =

walking and running, even- and uneven-surface; E3 = unperturbed and perturbed walking, young

5   and old). Motor primitives are the temporal coefficients of the four fundamental synergies for

locomotion. Lower FWHM imply shorter duration of activation.
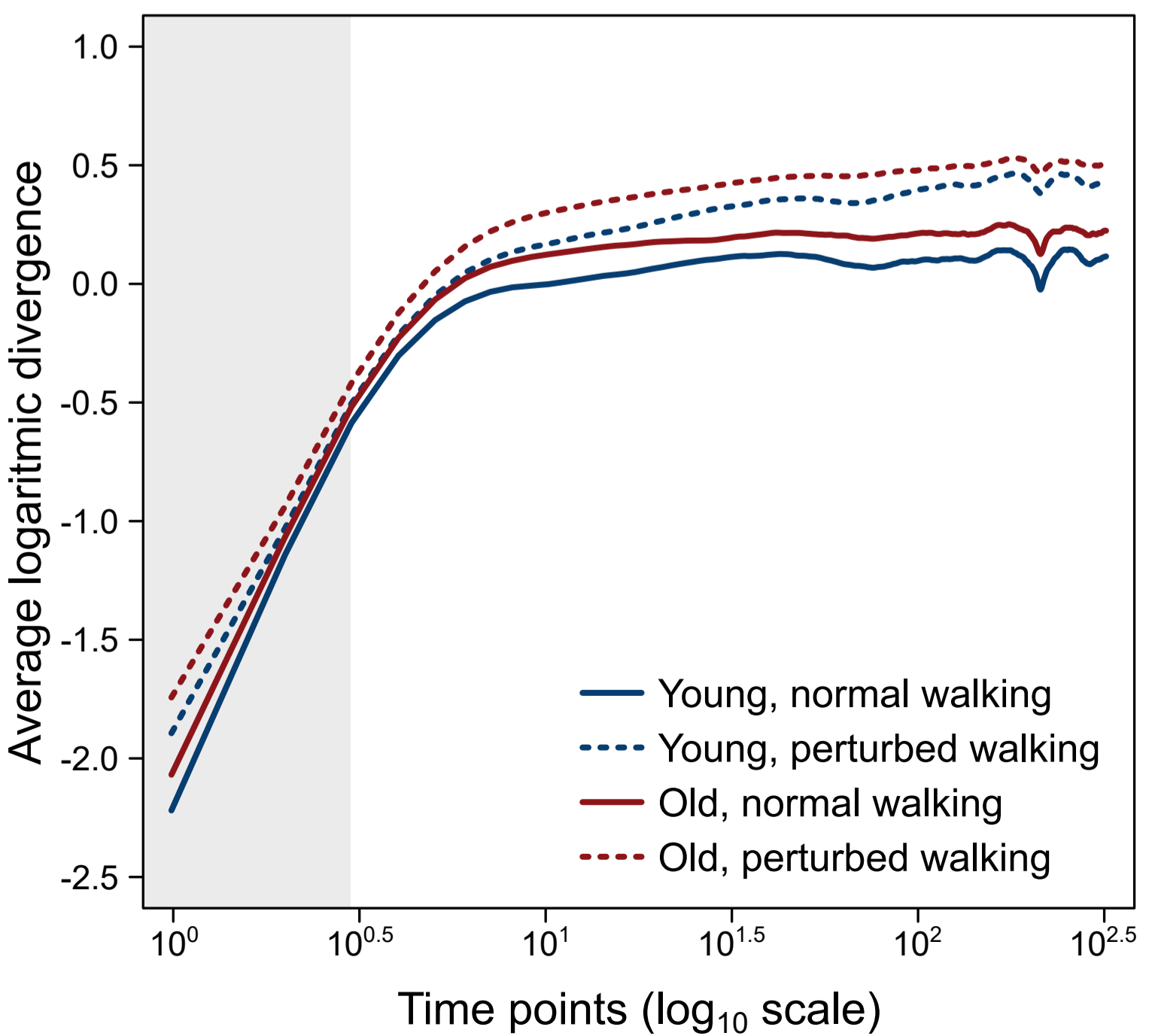
E1
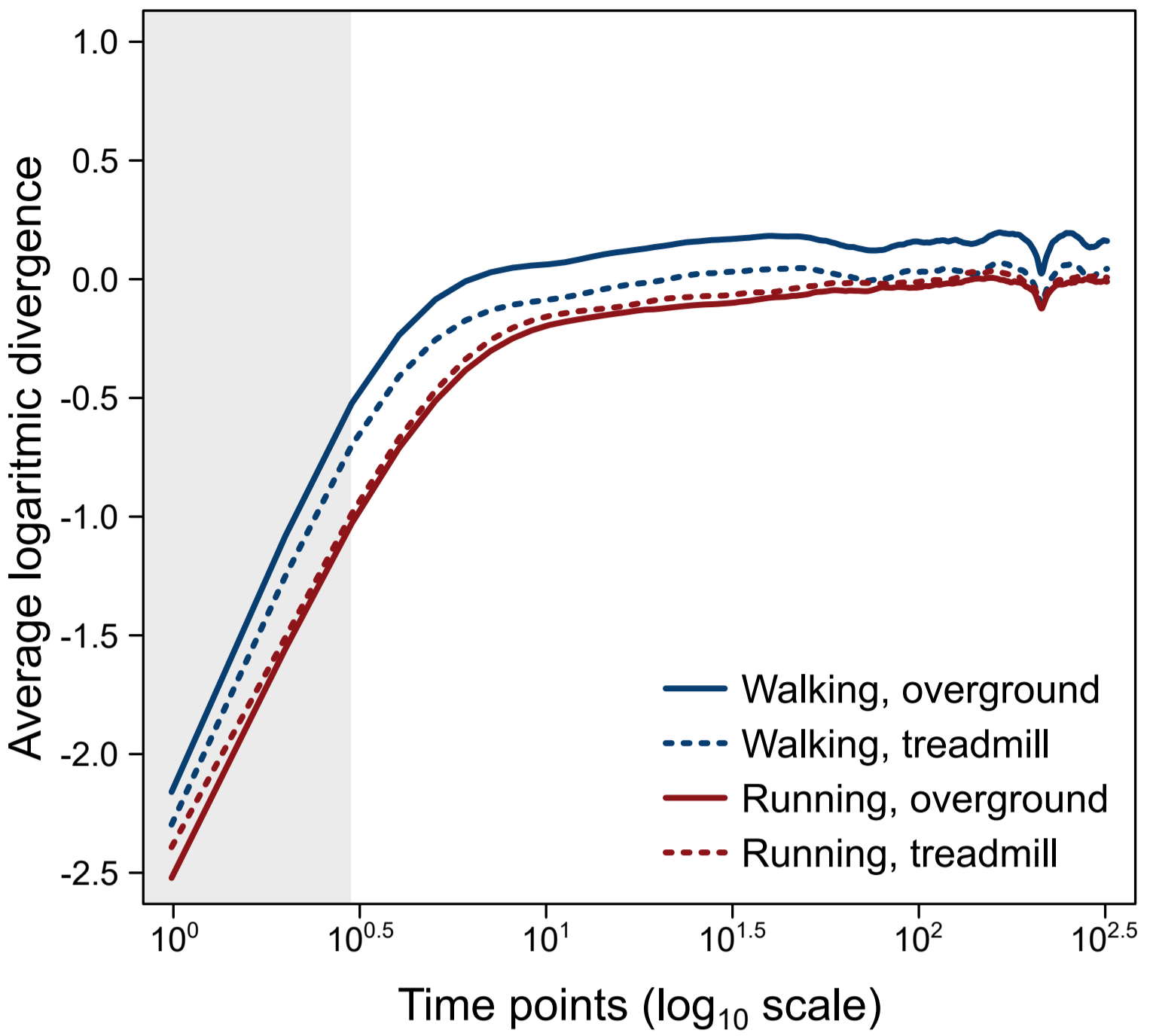
E2
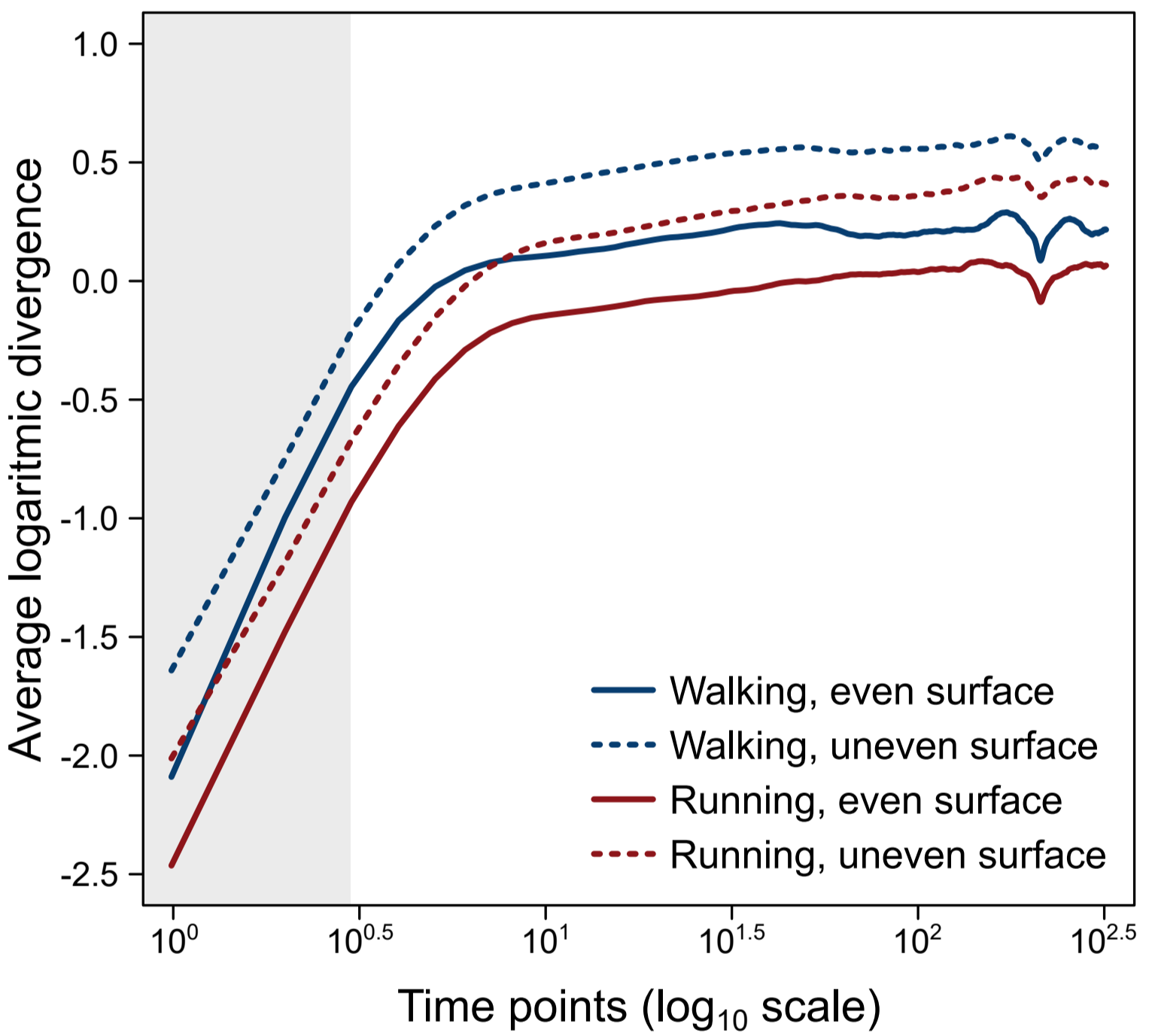
E3

Fig. S3. Average logarithmic divergence curves of motor primitives with their original vertical intercept related to Fig. 3. Curves describing the average logarithmic divergence curves for the three experimental setups (E1 = walking and running, overground and treadmill; E2 = walking and running, even- and uneven-surface; E3 = unperturbed and perturbed walking, young and old). The shaded area represents the portion considered for calculating the slope. Time is presented in $\log_{10}$ scale to highlight the curve slopes.

5

Supplemental references

Cappellini, G., Ivanenko, Y.P., Poppele, R.E., Lacquaniti, F., 2006. Motor patterns in human walking and running. J. Neurophysiol. 95, 3426–37. https://doi.org/10.1152/jn.00081.2006

Cheung, V.C.-K., D'Avella, A., Tresch, M.C., Bizzi, E., 2005. Central and sensory contributions to the activation and organization of muscle synergies during natural motor behaviors. J. Neurosci. 25, 6419–34. https://doi.org/10.1523/JNEUROSCI.4904-04.2005

D'Avella, A., Bizzi, E., 2005. Shared and specific muscle synergies in natural motor behaviors. Proc. Natl. Acad. Sci. U. S. A. 102, 3076–81. https://doi.org/10.1073/pnas.0500199102

Dingwell, J.B., Kang, H.G., Marin, L.C., 2007. The effects of sensory loss and walking speed on the orbital dynamic stability of human walking. J. Biomech. 40, 1723–30. https://doi.org/10.1016/j.jbiomech.2006.08.006

Dominici, N., Ivanenko, Y.P., Cappellini, G., D'Avella, A., Mondi, V., Cicchese, M., Fabiano, A., Silei, T., Di Paolo, A., Giannini, C., Poppele, R.E., Lacquaniti, F., 2011. Locomotor Primitives in Newborn Babies and Their Development. Science (80-.). 334, 997–999. https://doi.org/10.1126/science.1210617

Ekizos, A., Santuz, A., Schroll, A., Arampatzis, A., 2018. The Maximum Lyapunov Exponent During Walking and Running: Reliability Assessment of Different Marker-Sets. Front. Physiol. 9, 1101. https://doi.org/10.3389/fphys.2018.01101

Gizzi, L., Nielsen, J.F., Felici, F., Ivanenko, Y.P., Farina, D., 2011. Impulses of activation but not motor modules are preserved in the locomotion of subacute stroke patients. J. Neurophysiol. 106, 202–210. https://doi.org/10.1152/jn.00727.2010

Higuchi, T., 1988. Approach to an irregular time series on the basis of the fractal theory. Phys. D

Nonlinear Phenom. 31, 277–283. https://doi.org/10.1016/0167-2789(88)90081-4

Kantz, H., Schreiber, T., 2004. Nonlinear Time Series Analysis, 2nd ed. Cambridge University Press, Cambridge, UK.

Kesić, S., Spasić, S.Z., 2016. Application of Higuchi's fractal dimension from basic to clinical neurophysiology: A review. Comput. Methods Programs Biomed. 133, 55–70. https://doi.org/10.1016/j.cmpb.2016.05.014

Kloke, J.D., McKean, J.W., 2012. Rfit: Rank-based Estimation for Linear Models. R J. 4, 57–64.

Lee, D.D., Seung, H.S., 1999. Learning the parts of objects by non-negative matrix factorization. Nature 401, 788–91. https://doi.org/10.1038/44565

Lorenz, E.N., 1963. Deterministic Nonperiodic Flow. J. Atmos. Sci. 20, 130–141. https://doi.org/10.1175/1520-0469(1963)020<0130:DNF>2.0.CO;2

Maiwald, C., Sterzing, T., Mayer, T.A., Milani, T.L., 2009. Detecting foot-to-ground contact from kinematic data in running. Footwear Sci. 1, 111–118. https://doi.org/10.1080/19424280903133938

Martino, G., Ivanenko, Y.P., Serrao, M., Ranavolo, A., D'Avella, A., Draicchio, F., Conte, C., Casali, C., Lacquaniti, F., 2014. Locomotor patterns in cerebellar ataxia. J. Neurophysiol. 112, 2810–2821. https://doi.org/10.1152/jn.00275.2014

McKean, J.W., Kloke, J.D., 2014. Efficient and adaptive rank-based fits for linear models with skew-normal errors. J. Stat. Distrib. Appl. 1–18. https://doi.org/10.1186/s40488-014-0018-0

Packard, N.H., Crutchfield, J.P., Farmer, J.D., Shaw, R.S., 1980. Geometry from a Time Series. Phys. Rev. Lett. 45, 712–716. https://doi.org/10.1103/PhysRevLett.45.712

Rabinovich, M.., Abarbanel, H.D.., 1998. The role of chaos in neural systems. Neuroscience 87, 5–14. https://doi.org/10.1016/S0306-4522(98)00091-8

Rosenstein, M.T., Collins, J.J., De Luca, C.J., 1993. A practical method for calculating largest Lyapunov exponents from small data sets. Phys. D 65, 117–134. https://doi.org/10.1016/0167-2789(93)90009-P

Santuz, A., Akay, T., Mayer, W.P., Wells, T.L., Schroll, A., Arampatzis, A., 2019. Modular organization of murine locomotor pattern in the presence and absence of sensory feedback from muscle spindles. J. Physiol. 597, 3147–3165. https://doi.org/10.1113/JP277515

Santuz, A., Ekizos, A., Arampatzis, A., 2016. A Pressure Plate-Based Method for the Automatic Assessment of Foot Strike Patterns During Running. Ann. Biomed. Eng. 44, 1646–1655. https://doi.org/10.1007/s10439-015-1484-3

Santuz, A., Ekizos, A., Eckardt, N., Kibele, A., Arampatzis, A., 2018a. Challenging human locomotion: stability and modular organisation in unsteady conditions. Sci. Rep. 8, 2740. https://doi.org/10.1038/s41598-018-21018-4

Santuz, A., Ekizos, A., Janshen, L., Baltzopoulos, V., Arampatzis, A., 2017a. On the Methodological Implications of Extracting Muscle Synergies from Human Locomotion. Int. J. Neural Syst. 27, 1750007. https://doi.org/10.1142/S0129065717500071

Santuz, A., Ekizos, A., Janshen, L., Baltzopoulos, V., Arampatzis, A., 2017b. The Influence of Footwear on the Modular Organization of Running. Front. Physiol. 8, 958. https://doi.org/10.3389/fphys.2017.00958

Santuz, A., Ekizos, A., Janshen, L., Mersmann, F., Bohm, S., Baltzopoulos, V., Arampatzis, A., 2018b. Modular Control of Human Movement During Running: An Open Access Data Set.

Front. Physiol. 9, 1509. https://doi.org/10.3389/fphys.2018.01509

Sauer, T., Yorke, J.A., Casdagli, M., 1991. Embedology. J. Stat. Phys. 65, 579–616. https://doi.org/10.1007/BF01053745

Smits, F.M., Porcaro, C., Cottone, C., Cancelli, A., Rossini, P.M., Tecchio, F., 2016. Electroencephalographic Fractal Dimension in Healthy Ageing and Alzheimer's Disease. PLoS One 11, e0149587. https://doi.org/10.1371/journal.pone.0149587

Takens, F., 1981. Detecting strange attractors in turbulence, in: Rand, D., Young, L.-S. (Eds.), Dynamical Systems and Turbulence, Warwick 1980. Springer Berlin Heidelberg, Berlin, Heidelberg, pp. 366–381. https://doi.org/10.1007/BFb0091924

Theiler, J., 1990. Estimating the Fractal Dimension of Chaotic Time Series. Lincoln Lab. J. 3, 63–86. https://doi.org/10.1.1.229.3288